Application of an homogeneous model to simulate the heating of two-phase flows

Olivier Hurisse

Application of an homogeneous model to simulate the heating of two-phase flows.

Olivier Hurisse[†]

[†]*EDF R&D MFEE, 6 quai Watier, 78400 Chatou, France.*

olivier.hurisse@edf.fr

Abstract

This paper is dedicated to the simulation of two-phase flows on the basis of an homogeneous model that allows to account for the disequilibrium of the pressure, temperature and chemical potential (mass transfer). The numerical simulations are performed using a fractional step method treating separately the convective part of the model and the source terms. On the basis of analytical solutions for the convective part of the model, numerical investigations are performed to compare different finite volume schemes. Eventually, a test case of the heating of a mixture of steam and water is presented.

Key words : Homogeneous model, two-phase flows, mass transfer.

1 Introduction

In the nuclear domain, homogeneous models are often used to simulate the steam-water flows in devices such as the core, the steam-generator or other heat exchangers. One can for example cite, among others, the industrial codes THYC (EDF) [aub88, gue03], FLICA (CEA) [tou95] and ATHOS (EPRI) [ath07]. The homogeneous models deal with the flow as a mixture of the two phases. They are based on the Euler system of equations and then involve at least an equation for the mass conservation of the mixture, one for the momentum conservation of the mixture and one for the total energy of the mixture. These three PDE's can be supplemented by additional equations of transport of some fractions (most commonly one equation for the mass fraction of the mixture). The system of equations is then closed by providing an equation of state for the mixture [dow96, fau00] and, if necessary, closure laws for the source terms.

In a practical point of view, the homogeneous models are often obtained from two-fluid models [aub88, tou95]. The mixture equations for the mass, momentum

and energy are issued from the sum of the corresponding phasic equations of the two-fluid model. Algebraic closures are then proposed to get rid of the remaining phasic equations. If this process seems natural, it leads to some difficulties in defining the entropy of the system. More precisely, the entropy of the mixture is not always the sum of the phasic entropies. Another way of building an homogeneous model starting from a two-fluid model has been proposed in [gui05, sau08]. Asymptotic derivation has been performed and the resulting model leads to a model whose entropy is the sum of the phasic entropies. Nevertheless these models make the assumption of pressure equilibrium between the phases.

When no entropy can be exhibited, the second principle of thermodynamics might not hold, which could lead to non-physical behaviours of the model. This point is crucial when focusing on two-phase flows with phase change. In [bar05,hel06] a model built directly on the Euler system has been proposed. It is based on the second principle of thermodynamics and on additivity principles. The thermodynamical behaviour of the mixture and the thermodynamical exchanges between phases are then a straightforward consequence of these choices. Moreover, the resulting model is hyperbolic when two sufficient natural conditions hold for the equation of state for the entropy of each phase: the phasic entropies have to be concave with respect to the phasic specific volume and the phasic internal energy; and they must allow to define a positive thermodynamical temperature through the Gibbs relation.

In the classical homogeneous models, one assumes at least that the pressure equilibrium holds instantaneously ([kap01, ath07, aub88, tou95, dow96, fau00, gui05, sau08]). In addition to this hypothesis, the assumption is sometimes made that the mass transfer between the phases is instantaneous, leading to the so-called class of the Homogeneous Equilibrium Models (HEM). One can for example refer to [fac08, fac12, all07] where the thermodynamical equation of state for the mixture of the two phases is built by assuming the thermodynamical equilibrium between the phases. But in general, the homogeneous models do not account for the temperature disequilibrium [ath07, dow96, fau00, tou95, aub88] (the model proposed in [sau08] explicitely accounts for the temperature disequilibrium). The thermodynamical disequilibrium between the phases is a complex phenomenon and though it has been widely studied (see [bar05, hel06, mat10, hel11, jun13, fac08, fac12, all07, car04] among others), it remains difficult to handle.

The model proposed in [bar05, hel06] allows to account for the thermodynamical disequilibria between the phasic temperatures, the phasic pressures and the phasic chemical potentials. In this model, the time-space evolution of these equilibria is defined by three fractions (the volume, mass and energy fractions), each one being associated with an advection/source equation. The return to equilibrium is determined by the source terms, which are based on six quantities: one equilibrium value for each fraction and three time scales - characteristic of the time to return to equilibrium. The former are obtained from the entropy of the mixture and thus depend on the phasic equations of state, whereas the latter should be specified by the user - on the basis of physical considerations. The definition of the mixture of the two

phases through volume fration and mass fraction is classical ([kap01, gav07]) but the novelty of the model [bar05, hel06] is to define explicitely a third fraction to define the energy distribution between the phases. The authors then choose to express the return to equilibrium by defining three equilibrium fractions, as it is usually done for the sole mass fration ([fau00, dow96]). Classically these returns to equilibrium are expressed by source terms that are explicitely written in term of the pressure gap, temperature gap and chemical potential gap [gui05, sau08, kap01]. Nonetheless, the latter forms of source terms often imply the development of more complex and non-linear schemes to account for non-instantaneous or instantaneous relaxation of the equilibria.

Numerical simulations have been performed using the model proposed in [bar05]. The results of some test cases dedicated to cavitation phenomena show a good behaviour of the model [bar05]. In these simulations, an instantaneous temperature equilibrium has been imposed. This assumption is consistent with the cavitation phenomenon which is often seen as the creation of vapour due to a sudden pressure drop at an almost constant temperature. Our aim in the present paper is to test the behaviour of the model when considering test cases involving the heating of a mixture of steam and water. Indeed, these kinds of tests are representative of some nuclear situations such as: the heating of the primary coolant fluid by the fuel bundles, or the heating of the water in the steam generator device. Hence we do not assume any temperature equilibrium in the sequel.

The simulations are performed with a fractional step method [yan68]. We first account for the convective part of the system by using classical schemes: the Rusanov scheme [rus61], VFRoe-ncv schemes [mas99, gal96, buf00], and an energy relaxation method based on a VFRoe-ncv scheme [coq98]. The behaviour of these schemes is compared focusing on two Riemann problems described in appendix 6.1. The source terms are then taken into account through a straightforward integration which is made possible thanks to the form of the source terms.

The paper is organised as follows. On the basis of the paper [bar05] we first recall the model and its properties. Then, we propose a numerical scheme for the discretization of the model applied to stiffened gas equations of state. Eventually, an investigation is carried on an OECD/CSNI test case [csni80].

2 The homogeneous model

2.1 The system of equations

The velocity of the mixture is denoted by U, and since no kinematic disequilibrium is taken into account, U also represents the velocity of each phase. We note: $\rho = 1/\tau$ the density of the mixture, where τ is the specific volume, $E = e + U^2/2$ the specific total energy of the mixture, e the specific internal energy of the mixture, P the pressure in the mixture.

The fractions defining the manner in which the phases are mixed are denoted by $Y = (\alpha, y, z)^\top$ with $0 \leq Y^i \leq 1$, $i = 1..3$. The volume fraction $\alpha_l = \alpha$ represents the fraction of volume locally occupied by the liquid phase. Thanks to the volume conservation, $\alpha_v = 1 - \alpha$ represents the fraction of volume occupied by the vapour. As a consequence, if ρ_l and ρ_v are respectively the liquid and vapour density, the density of the mixture is then:

$$\rho = \alpha\rho_l + (1 - \alpha)\rho_v. \tag{1}$$

For each phase $k = l, v$ the mass fraction is defined as:

$$y_k = \alpha_k\rho_k/\rho,$$

and the energy fraction as:

$$z_k = y_k e_k/e.$$

Due to the relation (1), we have $y_l + y_v = 1$ and we then note $y = y_l$. We impose $z_l + z_v = 1$ and we note $z = z_l$. This is in fact equivalent to assuming that the internal energy of the mixture is the sum of the phasic internal energies weighted by the mass fractions:

$$e = ye_l + (1 - y)e_v. \tag{2}$$

We assume that the quantities ρ, U and E respectively fulfil the mass conservation equation, the momentum conservation equation and the equation for the total energy conservation. Moreover, we assume that the fractions are advected with the velocity U and are subject to source terms Γ_Y. We get then the following system of equations:

$$\begin{cases} \dfrac{\partial}{\partial t}(Y) + U\dfrac{\partial}{\partial x}(Y) = \Gamma_Y \\ \dfrac{\partial}{\partial t}(\rho) + \dfrac{\partial}{\partial x}(\rho U) = 0 \\ \dfrac{\partial}{\partial t}(\rho U) + \dfrac{\partial}{\partial x}\left(\rho U^2 + P\right) = 0 \\ \dfrac{\partial}{\partial t}(\rho E) + \dfrac{\partial}{\partial x}(\rho UE + UP) = 0. \end{cases} \tag{3}$$

Obviously, this system is not in a closed form, the equation of state for the mixture pressure $P = \mathcal{P}(Y, \rho, e)$ and the source terms $\Gamma_Y = (\Gamma_Y^1, \Gamma_Y^2, \Gamma_Y^3)^\top$ must be specified. This will be achieved in the following sections.

The entropy of the system (3) is a concave function s depending on Y, τ and e and is solution of the PDE:

$$\frac{\partial}{\partial \tau}(s) - P\frac{\partial}{\partial e}(s) = 0. \tag{4}$$

This constraint allows to ensure that s is advected with the velocity U without source terms (i.e. $\Gamma_Y = 0$). Obviously, the entropy is not unique and several forms might be proposed.

The differential of s reads:

$$ds(Y,\tau,e) = \frac{\partial}{\partial Y}(s)\ dY + \frac{\partial}{\partial \tau}(s)\ d\tau + \frac{\partial}{\partial e}(s)\ de,$$

or in another form:

$$\left(\frac{\partial}{\partial e}(s)\right)^{-1} ds(Y,\tau,e) = \left(\frac{\partial}{\partial e}(s)\right)^{-1} \frac{\partial}{\partial Y}(s)\ dY + \left(\frac{\partial}{\partial e}(s)\right)^{-1} \frac{\partial}{\partial \tau}(s)\ d\tau + de.$$

The classical Gibbs relation:

$$T\ ds = de + P\ d\tau + T\ \frac{\partial}{\partial Y}(s)\ dY,$$

can be retrieved by using (4) and by defining the thermodynamical temperature T and pressure P of the mixture through the entropy s:

$$T^{-1} = \frac{\partial}{\partial e}(s), \tag{5}$$

$$P = T\frac{\partial}{\partial \tau}(s) = \left(\frac{\partial}{\partial e}(s)\right)^{-1} \frac{\partial}{\partial \tau}(s). \tag{6}$$

In fact, the caloric law (definition of the temperature) and the equation of state for the pressure are fully defined by the definition of the mixture entropy s. This will be achieved in section 2.3. We now turn to the specification of the source terms Γ_Y which are obtained on the basis of the second law of thermodynamics.

2.2 Entropic characterisation of the source terms

We now use the second law of the thermodynamics to specify admissible forms for the source terms Γ_Y. By using the equations (3) and (4), it can be shown that when considering regular solutions the mixture entropy $s(Y,\tau,e)$ is ruled by the equation:

$$\frac{\partial}{\partial t}(s) + U\frac{\partial}{\partial x}(s) = \sum_i \frac{\partial}{\partial Y^i}(s)\ \Gamma_Y^i. \tag{7}$$

In order to ensure the non-decreasing of the entropy along all the streamlines, s and Γ_Y must be chosen such that:

$$\sum_i \frac{\partial}{\partial Y^i}(s)\ \Gamma_Y^i \geq 0, \forall (Y,\tau,e).$$

This specification remains general. We now choose a particular form for the source terms Γ_Y. For each fraction Y^i, we assume a classical "exponential" return to

equilibrium form defined by a characteristic time scale $\lambda^i > 0$ and an equilibrium value $Y^i_{eq}(\tau, e)$:

$$\Gamma^i_Y = \frac{Y^i_{eq}(\tau, e) - Y^i}{\lambda^i}, \tag{8}$$

This kind of form of source term is widely used in the literature, especially for homogeneous models [dow96, fau00]. Given the form (8) and using the property of the concavity of the entropy, we get:

$$\sum_i \frac{\partial}{\partial Y^i}(s)\ \Gamma^i_Y \geq \frac{s(Y_{eq}(\tau, e), \tau, e) - s(Y, \tau, e)}{\lambda^i}$$

As a consequence, the increase of the entropy is ensured if the equilibrium fractions are defined such that:

$$\forall(\tau, e),\ s(Y_{eq}(\tau, e), \tau, e) \geq s(Y, \tau, e).$$

In [bar05], the authors proposed to define Y_{eq} as the fractions realising the maximum of the entropy for a given specific volume τ and a given internal energy e, in other words:

$$s(Y_{eq}(\tau, e), \tau, e) = \max_{\{0 \leq Y \leq 1\}} (s(Y, \tau, e)). \tag{9}$$

This definition of Y_{eq} is of course in agreement with the second law of thermodynamics.

It is an important point to be noted that the source terms defined by (8) and (9) ensure the positivity of the fractions.

At this point of the paper, the entropy of the mixture s allows to close the system. The time scales λ^i are not defined but they should be specified by the user. Let us turn to the explicit choice of the entropy s.

2.3 Definition of the mixture entropy

We define now the entropy $s(Y, \tau, e)$ for the mixture following the approach of [bar05], but other choices might be possible. We assume that the thermodynamical behaviour of each phase is given by a phasic entropy $s_k = s_k(\tau_k, e_k)$. Each phasic entropy allows to define a phasic caloric law

$$T_k^{-1} = \frac{\partial}{\partial e_k}(s_k), \tag{10}$$

and a phasic pressure law

$$P_k = T_k \frac{\partial}{\partial \tau_k}(s_k), \tag{11}$$

in agreement with the definitions (5) and (6). We then write the mixture entropy as the mixing of the two phasic entropies:

$$\begin{aligned} s(\tau, e, Y) &= y s_l(\tau_l, e_l) + (1-y) s_v(\tau_v, e_v) \\ &= y s_l(\tfrac{\alpha}{y}\tau, \tfrac{z}{y}e) + (1-y) s_v(\tfrac{1-\alpha}{1-y}\tau, \tfrac{1-z}{1-y}e). \end{aligned} \tag{12}$$

This proposition is classical for mixtures of non-miscible phases, since the entropy of the union of two systems is the addition of the entropies of each system. Moreover, if the entropies $s_k = s_k(\tau_k, e_k)$ are concave with respect to (τ_k, e_k) and if they do not coincide, then the mixture entropy (12) is also concave with respect to the fractions Y (see [hel06,jun13] or appendix 6.4 for details). This property is mandatory to define a unique Y_{eq} using (9). The mixture entropy is also concave with respect to the variable (τ, e) (see [hel06,jun13] or appendix 6.4 for details).

Once the phasic entropy functions $(\tau_k, e_k) \to s_k(\tau_k, e_k)$ and the time scales λ_i are chosen, the whole system is closed and we can then study its properties.

2.4 Properties of the model

Given the mixture entropy (12), the mixture temperature (5) and the mixture pressure (6) can be explicitly written in term of the phasic temperatures (10) and pressures (11):

$$P = \frac{\alpha T}{T_l} P_l + \frac{(1-\alpha)T}{T_v} P_v \quad \text{and} \quad \frac{1}{T} = \frac{z}{T_l} + \frac{1-z}{T_v}. \tag{13}$$

The mixture temperature is a geometric barycenter of the phasic temperatures. Moreover, the pressure is not a barycenter of the phasic pressures, excepted in the single-phase situations which is a degenerate situation. Indeed it can be written:

$$P = \frac{\frac{\alpha}{T_l} P_l + \frac{(1-\alpha)}{T_v} P_v}{\frac{z}{T_l} + \frac{1-z}{T_v}}.$$

The equilibrium fractions are implicitly defined by the maximisation of the mixture entropy (9). When the maximum is not reached on the boundary of the domain, i.e. when $0 < Y_{eq} < 1$, the gradient of s with respect to Y evaluated at $Y = Y_{eq}$ equals zero:

$$\frac{\partial}{\partial \alpha}(s)_{|Y=Y_{eq}} = \frac{\partial}{\partial y}(s)_{|Y=Y_{eq}} = \frac{\partial}{\partial z}(s)_{|Y=Y_{eq}} = 0.$$

By using the definition (12), this yields:

$$\frac{\partial}{\partial \alpha}(s)_{|Y=Y_{eq}} = 0 \Leftrightarrow \tau \left(\frac{P_l}{T_l} - \frac{P_v}{T_v} \right) = 0, \tag{14}$$

$$\frac{\partial}{\partial z}(s)_{|Y=Y_{eq}} = 0 \Leftrightarrow e \left(\frac{1}{T_l} - \frac{1}{T_v} \right) = 0, \tag{15}$$

$$\frac{\partial}{\partial y}(s)_{|Y=Y_{eq}} = 0 \Leftrightarrow - \left(\frac{\mu_l}{T_l} - \frac{\mu_v}{T_v} \right) = 0, \tag{16}$$

with the chemical potentials $\mu_k = e_k + P_k \tau_k - T_k s_k$. The fraction Y_{eq} is thus the solution of the non-linear system:

$$\begin{cases} T_l(\tau, e, Y_{eq}) = T_v(\tau, e, Y_{eq}) \\ P_l(\tau, e, Y_{eq}) = P_v(\tau, e, Y_{eq}) \\ \mu_l(\tau, e, Y_{eq}) = \mu_v(\tau, e, Y_{eq}). \end{cases} \tag{17}$$

This system only makes sense when the maximum of the entropy is reached inside the two-phase domain $0 < Y_{eq} < 1$. When the maximum is reached on the boundary of the domain, the equalities in (17) become inequalities. Hence definition (9) should be used to define Y_{eq}: we then have $Y_{eq} = 0$ if $s(0, \tau, e) > s(1, \tau, e)$ or $Y_{eq} = 1$ if $s(0, \tau, e) < s(1, \tau, e)$.

Remark. Note that when considering stiffened gas EOS, the system (17) can have a solution with one or two equilibrium fractions equal to zero and the other lying in $]0, 1[$. Such a case is described in appendix 6.2 and more detailed explanations can be found in [jun13].

The sound speed c for the system (3) is defined as:

$$c^2 = -\tau^2 \frac{\partial}{\partial \tau}(P)_{|s} = -\tau^2 \frac{\partial}{\partial \tau}(P) + \tau^2 P \frac{\partial}{\partial e}(P),$$

and using the formula (13) it can be written:

$$\frac{c^2}{T\tau^2} = -(-\alpha, Pz).s_l''.\begin{pmatrix} -\alpha \\ Pz \end{pmatrix} - (-(1-\alpha), P(1-z)).s_v''.\begin{pmatrix} -(1-\alpha) \\ P(1-z) \end{pmatrix} \quad (18)$$

where s_k'' stands for the Hessian matrix of the phasic entropies $(\tau_k, e_k) \to s_k(\tau_k, e_k)$. We recall that the phasic sound speeds are defined as:

$$\frac{c_k^2}{T_k \tau_k^2} = -(-1, P).s_k''.(-1, P)^\top \quad (19)$$

It must be emphasised that the mixture celerity c is not a barycenter of the phasic celerities c_k. Some empiric formulations and some experiments tend to confirm this behaviour for c [kar58, wal69, liu13]. Moreover, two natural sufficient conditions can be expressed for the celerity c to be defined in the real space. If:

- each phasic entropy is concave with respect to the phasic specific volume and to the phasic specific internal energy,
- and the mixture temperature is positive,

then c^2 is non-negative, and hence c is real. These conditions are sufficient and not necessary. With the present model, the mixture sound speed can be defined even if one of the phasic celerities is not defined and/or if one phasic temperature is not positive.

The eigenstructure of system (3) is the same as the eigenstructure of the Euler system. The fields associated with the fractions Y^i are linearly degenerated and the corresponding eigenvalue is U. The mass, momentum, energy sub-system yields the eigenvalues U and $U \pm c$. The former is associated with a linearly degenerated field, while the latter are genuinely non-linear waves.

Thanks to the form of the equations for the fractions Y and thanks to the equilibrium fractions Y_{eq} which, by definition, lie in $[0, 1]$, the positivity of the fractions is ensured.

3 Numerical schemes

We propose herein a finite volume scheme to simulate the model defined in the previous section. The general scheme relies on a classical fractional step method [yan68]: we first account for the convective part of the system (3) and then the source terms for the fractions are discretised. The latter step involves the computation of the equilibrium fractions Y_{eq}.

3.1 The Stiffened Gas EOS

In order to avoid numerical difficulties and to diminish the computational cost in the computation of the equilibrium fractions, we focus on the stiffened gas equations of state. This class of equation of state allows to obtain a rather satisfactory behaviour for the liquid phase, and it degenerates naturally to the perfect gas equation of state for the steam. The phasic entropies are then:

$$s_k(\tau_k, e_k) = C_{v,k} \ln\left((e_k - \Pi_k \tau_k)\tau_k^{\gamma_k - 1}\right) + s_k^0, \tag{20}$$

where $\Pi_k > 0$, and:

- $C_{v,k}$ is the heat capacity,
- $-\Pi_k$ is the minimal pressure (the phasic entropy and the phasic sound speed are defined for $P_k > -\Pi_k$; and the phasic temperature is positive for $P_k > -\Pi_k$),
- $\gamma_k > 1$ is the adiabatic coefficient,
- s_k^0 is the reference entropy.

The phasic pressure and phasic temperature laws are respectively given by (11) and (10), and for stiffened gas it yields:

$$P_k(\tau_k, e_k) = \frac{e_k}{\tau_k}(\gamma_k - 1) - \Pi_k \gamma_k, \quad \text{or} \quad P_k(\tau, e, Y) = \frac{z_k}{\alpha_k}\frac{e}{\tau}(\gamma_k - 1) - \Pi_k \gamma_k, \tag{21}$$

$$T_k(\tau_k, e_k) = \frac{e_k - \Pi_k \tau_k}{C_{v,k}}, \quad \text{or} \quad T_k(\tau, e, Y) = \frac{\frac{z_k}{y_k} e - \Pi_k \frac{\alpha_k}{y_k}\tau}{C_{v,k}}. \tag{22}$$

The thermodynamical variables of the system are (Y, τ, e). In the previous section the thermodynamical pressure has been defined using these variables, so that the calculus of (Y, τ, P) is straightforward when (Y, τ, e) is known. In general, the inverse variables change $(Y, \tau, P) \to (Y, \tau, e)$ is not straightforward. In the particular case of the stiffened gas EOS, an explicit variable change can be exhibited. By replacing the definition of the phasic pressure (21) and the phasic temperature (22) in the the definition of the mean pressure (13), a second degree polynomial in e can be formed:

$$A(Y, \tau, P)\ e^2 + B(Y, \tau, P)\ e + C(Y, \tau, P) = 0, \tag{23}$$

with the coefficients:

$$\begin{aligned}
A(Y,\tau,P) &= z(1-z)\tfrac{1}{\tau}\left(\alpha C_{v,l}(\gamma_l-1)+(1-\alpha)C_{v,v}(\gamma_v-1)\right),\\
B(Y,\tau,P) &= -Pz(1-z)(yC_{v,l}+(1-y)C_{v,v})\\
&\quad -\alpha C_{v,l}\left((1-\alpha)z(\gamma_l-1)\Pi_v+y(1-z)\gamma_l\Pi_l\right)\\
&\quad -(1-\alpha)C_{v,v}\left(\alpha(1-z)(\gamma_v-1)\Pi_l+(1-y)z\gamma_v\Pi_v\right),\\
C(Y,\tau,P) &= \alpha(1-\alpha)\Pi_l\Pi_v\tau\left(yC_{v,l}\gamma_l+(1-y)C_{v,v}\gamma_v\right)\\
&\quad +P\tau\left((1-\alpha)yzC_{v,l}\Pi_v+\alpha(1-y)(1-z)C_{v,v}\Pi_l\right).
\end{aligned}$$

For any non-negative pressure, $P>0$, this polynomial has always two non-negative solutions, and the smallest solution equals zero in the case of perfect gases $\Pi_k=0$. We thus retain the greatest solution as the unique physical solution. When the pressure is negative, no general result has been exhibited. Hence, if (Y,τ,P) is known with $P>0$, (Y,τ,e) can be explicitly computed. This variable change will be useful in the convection step and in the computation of an analytical solution through the Hugoniot curve (see appendix 6.1).

3.2 The convection step

The convective part of the system (3) is based on the Euler system of equations and a lot of Finite Volume schemes can be found in the literature to obtain numerical approximations of its solutions. The main difficulty here lies in the complexity of the equations of state. A strong jump of the fractions Y may lead to an important jump in the thermodynamical functions which may lead to numerical difficulties on coarse meshes as described in [gal02a]. In order to achieve this step, four different first-order schemes have been tested here:

(i) the classical Rusanov scheme [rus61];

(ii) the VFRoe-ncv scheme [buf00] using the variables (Y,τ,U,e) with the entropic correction [hel10];

(iii) the VFRoe-ncv scheme using the variables (Y,τ,U,P) [buf00] with the entropic correction [hel10];

(iv) the VFRoe-ncv scheme using the variables (Y,τ,U,P) and the energy relaxation method [coq98, gal02a].

Despite its poor accuracy, the Rusanov scheme remains a reference scheme because it is very easy to implement and very robust. The VFRoe-ncv schemes form a class of accurate schemes. Depending on the choice of the non-conservative variables, interesting properties can be obtained [gal96, gal02a, gal03]. In particular, when choosing U and P, it allows to preserve unsteady contact discontinuities for a specific class of EOS [gal02b]. The last scheme (iv) is based on the VFRoe-ncv scheme but it uses a relaxation of the EOS that is very convenient for the systems that possess a complex EOS.

We set $W = (Y, \rho, \rho U, \rho E)$ and $\mathcal{F} : W \mapsto (\rho Y, \rho U, \rho U^2 + P, \rho UE + UP)$. For any quantity Φ, Φ_i^n stands for the Finite Volume [eym00] approximation of Φ in the cell i at time t^n. For the sake of simplicity, we assume that all the cells have the same size Δx. The time step $\Delta t^n = t^{n+1} - t^n$ is chosen in agreement with a CFL condition that depends on the scheme. For an approximation W_j^n of W at time t^n and in the cell j, the approximation $W_j^{n+1,*}$ at the end of the convection step is computed by the scheme:

$$W_i^{n+1,*} - W_i^n + \frac{\Delta t^n}{\Delta x}\left(F(W_{i+1}^n, W_i^n) - F(W_i^n, W_{i-1}^n)\right) = 0, \tag{24}$$

$F(.,.)$ is the two-point numerical flux and it is described for each scheme in the sections below.

3.2.1 The Rusanov scheme

For the Rusanov scheme, we have:

$$F(W_l, W_r) = \frac{1}{2}\left(\mathcal{F}(W_l) + \mathcal{F}(W_r)\right) - \frac{\max\left(\Lambda_r, \Lambda_l\right)}{2}(W_r - W_l), \tag{25}$$

where Λ_r (resp. Λ_l) denotes the spectral radius of the convection matrix $\nabla_W \mathcal{F}$ at $W = W_r$ (resp. $W = W_l$). The time step Δt^n must fulfil the CFL constraint:

$$\frac{\Delta t^n}{\Delta x}\max\left(\Lambda_r, \Lambda_l\right) < 1/2.$$

3.2.2 The VFRoe-ncv scheme

Let us note V a set of variables such that a variable change Φ (diffeomorphism) exists with: $W = \Phi(V)$ and $V = \Phi^{-1}(W)$. For regular solutions, the convective part of the system (3) can be written in a non-conservative form using the variable V:

$$\frac{\partial}{\partial t}(V) + A(V)\frac{\partial}{\partial x}(V) = 0,$$

where $A = (\nabla_V \Phi)^{-1}(\nabla_W \mathcal{F})(\nabla_V \Phi)$ is the convection matrix. The numerical flux for the VFRoe-ncv scheme then reads:

$$F(W_l, W_r) = \mathcal{F}(\Phi(\mathcal{V}(x/t = 0, \Phi^{-1}(W_l), \Phi^{-1}(W_r)))), \tag{26}$$

where $\mathcal{V}(x/t, V_l, V_r)$ is the exact solution of the Riemann problem associated with the system:

$$\frac{\partial}{\partial t}(V) + A(\overline{V})\frac{\partial}{\partial x}(V) = 0, \text{ with } \overline{V} = (V_l + V_r)/2 \tag{27}$$

and with the left state V_l and the right state V_r. The time step Δt^n must fulfil:

$$\frac{\Delta t^n}{\Delta x}\Lambda_{l,r} < 1/2.$$

where $\Lambda_{l,r}$ is the spectral radius of $A(\overline{V})$.

The scheme using the flux (26) can converge towards a wrong solution because of the occurrence of non-entropic shocks in the fan of a rarefaction wave that crosses $x/t = 0$. In order to ensure the convergence towards the right solution a simple entropic correction has been proposed in [hel10]. It consists in modifying the flux (26) by adding a diffusive term:

$$F(W_l, W_r) = \mathcal{F}(\Phi(\mathcal{V}(x/t = 0, \Phi^{-1}(W_l), \Phi^{-1}(W_r)))) - \frac{\delta}{2}(W_r - W_l). \qquad (28)$$

The correction coefficient δ is equal to: $\delta = \min(-(U+c)_l, (U+c)_r)$ when $(U+c)_l < 0$ and $(U+c)_r > 0$; $\delta = \min(-(U-c)_l, (U-c)_r)$ when $(U-c)_l < 0$ and $(U-c)_r > 0$; otherwise $\delta = 0$. Hence the additional diffusive term is activated only if necessary, and does not decrease the global accuracy of the scheme.

In the sequel we have chosen two different sets of variables for V, leading to two different schemes. With the first choice $V = (Y, \tau, U, e)$ the resulting convection matrix has a lot of non-zero terms with a complex expression. Whereas with the second choice, $V = (Y, \tau, U, P)$, the convection matrix is more sparse and the expressions associated with the solution of the linearised Riemann problem (27) are simpler. Moreover, it has been shown in [gal02b] that choosing U and P in the set a variables V ensure the preservation of an unsteady contact discontinuity, provided that the equation of state is of the form:

$$\rho e = \rho \mathcal{G}_1(P) + \rho\alpha \mathcal{G}_2(P) + \rho y \mathcal{G}_3(P) + \rho z \mathcal{G}_4(P) + \mathcal{G}_5(P).$$

Unfortunately, in the present case, the internal energy (23) can not be written in the form above.

An important point to be quoted is that it is mandatory to express the internal energy with respect to (Y, τ, P) (23) in order to compute (26) for the choice $V = (Y, \tau, U, P)$.

3.2.3 The VFRoe-ncv scheme with energy relaxation

This scheme is based on a VFRoe-ncv (Y, τ, U, P) scheme [buf00] with a method of relaxation for the energy [coq98] that allows to account for complex EOS. In [gal02a] the complex EOS is replaced by a perfect gas EOS and the pressure must then remain positive. With the complex EOS described in the section above, the pressure may become negative and the scheme [gal02a] should be modified by introducing another parameter Π to replace the perfect gas EOS by a stiffened gas EOS.

As in [gal02a] we define Γ_1 and Γ_2 such that:

$$\Gamma_1 = \max_{(i)} \left(1 + \tau_i \frac{\partial}{\partial e}(P)(Y_i, \tau_i, e_i)\right),$$

and

$$\Gamma_2 = \max_{(i)} \left(-\frac{\tau_i}{P_i}\frac{\partial}{\partial \tau}(P)(Y_i, \tau_i, e_i) + \tau_i \frac{\partial}{\partial e}(P)(Y_i, \tau_i, e_i)\right),$$

and we choose $\Gamma > \max(\Gamma_1, \Gamma_2)$ (in practice we have chosen $\Gamma = 1.01 \times \max(\Gamma_1, \Gamma_2)$). A modified energy ϵ is introduced:

$$\epsilon = e - \left(\tau \frac{P}{\Gamma - 1}\right)$$

as well as the system:

$$\frac{\partial}{\partial t}\left(W^{\#}\right) + \frac{\partial}{\partial x}\left(\mathcal{F}^{\#}(W^{\#})\right) = 0, \tag{29}$$

with

$$W^{\#} = \left(\rho Y, \rho, \rho U, \frac{\rho U^2}{2} + \frac{P}{\Gamma - 1}, \rho\epsilon\right)$$

and

$$\mathcal{F}^{\#}(W^{\#}) = \left(\rho U Y, \rho U, \rho U^2 + P, U\frac{\rho U^2}{2} + U\frac{\Gamma P}{\Gamma - 1}, \rho U \epsilon\right).$$

System (29) corresponds to system (3) (without the source terms) for a perfect gas EOS with parameter Γ, supplemented by an advection equation for ϵ.

If $F_j^{\#,VFRoe}(W_l^{\#}, W_r^{\#})$, $j = 1..5$, stands for the j^{th} component of the VFRoe-ncv $(Y, \tau, U, P, \epsilon)$ flux described above (26) for system (29), F_j the j^{th} component of flux corresponding to the Coquel-Perthame energy relaxation scheme is:

$$\begin{aligned}
F_1(W_l, W_r) &= F_1^{\#,VFRoe}(W_l^{\#}, W_r^{\#}),\\
F_2(W_l, W_r) &= F_2^{\#,VFRoe}(W_l^{\#}, W_r^{\#}),\\
F_3(W_l, W_r) &= F_3^{\#,VFRoe}(W_l^{\#}, W_r^{\#}),\\
F_4(W_l, W_r) = F_4^{\#,VFRoe}(W_l^{\#}, W_r^{\#}) &+ F_5^{\#,VFRoe}(W_l^{\#}, W_r^{\#}).
\end{aligned}$$

Three important points must be emphasised:

(i) this scheme does not need an entropy correction, the fluxes $F^{VFRoe}(W_l, W_r)$ are computed with (26) and it is not mandatory to use fluxes (28);

(ii) the computation of the internal energy with respect to (Y, τ, U, P) (23) is not needed (this is the case for the VFRoe-ncv (Y, τ, U, P) without energy relaxation, see the section 3.2.2).

(iii) In [bar05], the temperature equilibrium is enforced and the resulting mixture pressure EOS is a Stiffend Gas EOS. The Coquel-Perthame relaxation procedure is then unnecessary in that case.

3.3 The source terms step

The source terms of the system (3) are accounted for by discretising the system of ODE:

$$\left\{\begin{array}{l} \dfrac{\partial}{\partial t}(\alpha) = \dfrac{\alpha_{eq}(\tau,e)-\alpha}{\lambda^{(1)}} \\ \dfrac{\partial}{\partial t}(y) = \dfrac{y_{eq}(\tau,e)-y}{\lambda^{(2)}} \\ \dfrac{\partial}{\partial t}(z) = \dfrac{z_{eq}(\tau,e)-z}{\lambda^{(3)}} \\ \dfrac{\partial}{\partial t}(\rho) = 0 \\ \dfrac{\partial}{\partial t}(\rho U) = 0 \\ \dfrac{\partial}{\partial t}(\rho E) = 0 \end{array}\right. \tag{30}$$

We first remark that it can be written in an equivalent manner:

$$\left\{\begin{array}{l} \dfrac{\partial}{\partial t}(\alpha(t)) = \dfrac{\alpha_{eq}(\tau(0),e(0))-\alpha(t)}{\lambda^{(1)}(t)} \\ \dfrac{\partial}{\partial t}(y(t)) = \dfrac{y_{eq}(\tau(0),e(0))-y(t)}{\lambda^{(2)}(t)} \\ \dfrac{\partial}{\partial t}(z(t)) = \dfrac{z_{eq}(\tau(0),e(0))-z(t)}{\lambda^{(3)}(t)} \\ \dfrac{\partial}{\partial t}(\tau(t)) = 0 \\ \dfrac{\partial}{\partial t}(U(t)) = 0 \\ \dfrac{\partial}{\partial t}(e(t)) = 0 \end{array}\right. \tag{31}$$

It can thus be noticed that if the parameters $\lambda^{(j)}$ are constant, the system (31) can be integrated exactly. We then approach system (31) by replacing $\lambda^{(j)}(t)$ by its value $\lambda^{(j)}(0)$. It yields for the fractions:

$$\left\{\begin{array}{l} \dfrac{\partial}{\partial t}(\alpha(t)) = \dfrac{\alpha_{eq}(\tau(0),e(0))-\alpha(t)}{\lambda^{(1)}(0)} \\ \dfrac{\partial}{\partial t}(y(t)) = \dfrac{y_{eq}(\tau(0),e(0))-y(t)}{\lambda^{(2)}(0)} \\ \dfrac{\partial}{\partial t}(z(t)) = \dfrac{z_{eq}(\tau(0),e(0))-z(t)}{\lambda^{(3)}(0)} \end{array}\right. \tag{32}$$

The numerical approximation W^{n+1} is the exact solution of the system (32) at time $t = \Delta t$ and with the initial condition $W^{n+1,*}$, the values obtained after the

convection step. The final approximation W^{n+1} then reads:

$$\left\{\begin{array}{l} \alpha^{n+1} = e^{(-\Delta t/\lambda^{(1),n+1,*})}\alpha^{n+1,*} - \alpha_{eq}^{n+1,*}\left(e^{(-\Delta t/\lambda^{(1),n+1,*})} - 1\right) \\ y^{n+1} = e^{(-\Delta t/\lambda^{(2),n+1,*})}y^{n+1,*} - y_{eq}^{n+1,*}\left(e^{(-\Delta t/\lambda^{(2),n+1,*})} - 1\right) \\ z^{n+1} = e^{(-\Delta t/\lambda^{(3),n+1,*})}z^{n+1,*} - z_{eq}^{n+1,*}\left(e^{(-\Delta t/\lambda^{(3),n+1,*})} - 1\right) \\ \rho^{n+1} = \rho^{n+1,*} \\ U^{n+1} = U^{n+1,*} \\ e^{n+1} = e^{n+1,*} \end{array}\right. \tag{33}$$

Remark. If the time scales λ_i only depend on e and τ, system (32) is equivalent to the first three equations of (31) and scheme (33) corresponds to an exact integration. But when the time scales depend on the fractions, the exact integration might become impossible.

It now remains to compute the equilibrium fractions α_{eq}, y_{eq} and z_{eq} for a given couple (τ, e). In the particular case of the stiffened gas EOS, the non-linear system (17) for Y_{eq} can be reduced to a resolvant equation on the fraction α_{eq}. Indeed, the pressure equilibrium $P_l(\tau, e, Y_{eq}) = P_v(\tau, e, Y_{eq})$ gives an explicit expression of z_{eq} with respect to α_{eq}:

$$z_{eq}(\alpha_{eq}) = \frac{\alpha_{eq}(\gamma_v - 1) - \alpha_{eq}(1-\alpha_{eq})(\Pi_v\gamma_v - \Pi_l\gamma_l)\tau/e}{\alpha_{eq}(\gamma_v - 1) + (1-\alpha_{eq})(\gamma_l - 1)},$$

and the temperature equilibrium $T_l(\tau, e, Y_{eq}) = T_v(\tau, e, Y_{eq})$ gives an explicit expression of y_{eq} with respect to α_{eq} and z_{eq}:

$$y_{eq}(\alpha_{eq}, z_{eq}) = \frac{(ez_{eq} - \Pi_l\alpha_{eq}\tau)/C_{v,l}}{(ez_{eq} - \Pi_l\alpha_{eq}\tau)/C_{v,l} + (e(1-z_{eq}) - \Pi_l(1-\alpha_{eq})\tau)/C_{v,v}}.$$

Finally, the equilibrium of the chemical potentials can then be written as a non-linear equation on α_{eq}:

$$\begin{array}{l} \mu_l(\tau,\ e,\ \alpha_{eq},\ y_{eq}(\alpha_{eq}, z_{eq}(\alpha_{eq})),\ z_{eq}(\alpha_{eq})) \\ \qquad = \mu_v(\tau,\ e,\ \alpha_{eq},\ y_{eq}(\alpha_{eq}, z_{eq}(\alpha_{eq})),\ z_{eq}(\alpha_{eq})). \end{array} \tag{34}$$

In practice, equation (34) is solved using a dichotomy algorithm. If the dichotomy algorithm fails finding a zero for (34), the two phases do not co-exist for (τ, e). We then use definition (9) to determine Y_{eq}: $Y_{eq} = 0$ if $s(\tau, e, 0) > s(\tau, e, 1)$; and $Y_{eq} = 1$ if $s(\tau, e, 0) < s(\tau, e, 1)$.

For more complex EOS it could be more convenient to compute the equilibrium fractions by using definition (9) and an optimisation algorithm instead of solving (17).

4 Numerical simulations

4.1 Comparison of the behaviour of the convection schemes

We first verify the numerical schemes of section 3.2 by using the two Riemann problems described in appendix 6.1. The results computed with the different schemes

are obtained with the same CFL constraint of 0.45.

4.1.1 Test case with initial conditions of table (13)

The approximations obtained by the four schemes have been compared with the analytical solution (see appendix 6.1 for details) in terms of the L_1 error:

$$err(\phi, T) = \frac{\sum_{i=1}^{N} |\phi^{approx}(T, x_i) - \phi^{exact}(T, x_i)|}{\sum_{i=1}^{N} |\phi^{exact}(T, x_i)|}, \tag{35}$$

where N stands for the number of cells on $[0, 1]$, x_i is the centre of the cell i and T is the final time (here $T = 0.001\ s$). The CFL number is equal to 0.45, except in the first time steps where it increases from 0.05 to 0.45. The mesh size is uniform $\Delta x = 1/N$, and different values for N have been used: $N = \{10^2, 5\ 10^2, 10^3, 5\ 10^3, 10^4, 5\ 10^4, 10^5\}$. Due to the important oscillations observed in the approximations of the VFRoe-ncv (Y, τ, U, e) scheme for coarse meshes, it has been necessary to increase the number of cells to $N = \{2\ 10^5, 5\ 10^5, 10^6\}$ in order to recover the asymptotic convergence rate. These oscillations are stable in L_1-norm and L^∞-norm with respect to the mesh size. On coarse meshes, $N < 10^5$ for the present test case, they appear in the ghost wave region and in front of the discontinuities. The error (35) has been plotted on figure (1). It can be seen that we get the expected convergence rate of 1/2 due to the presence of the contact wave [gal02a].

The approximations are plotted on figures (2), (3) and (4) for respectively $N = 10^3$, $N = 10^5$ and $N = 10^6$ with a zoom on the ghost wave location. Numerical approximations obtained with the four schemes contain perturbations around the expected ghost-wave except for the fractions Y. VFRoe-ncv (Y, τ, U, e) and Rusanov schemes are indeed sensitive whereas the two VFRoe-ncv (Y, τ, U, P) provide smaller overshoots. Concerning the preservation of the unsteady contact discontinuity for U and P, the two latter schemes have a satisfactory behaviour even if the EOS does not allow an exact preservation. However, the results obtained with the VFRoe-ncv (Y, τ, U, e) exhibit strong peaks and/or oscillations in the vicinity of the contact wave at the front location of the shock. This is particularly true on coarse meshes, which explains the very poor accuracy for U, ρ and P. Nevertheless the magnitude of the peaks and oscillations decreases when the mesh size decreases.

The computational efficiency of the different schemes has been investigated by plotting the error (35) with respect to the CPU time in seconds. The results can be seen on figure (5). The first remark is that the Rusanov scheme has a very poor efficiency in comparison with the VFRoe-ncv (Y, τ, U, P) schemes (with or without the energy relaxation). Nevertheless, it remains interesting versus the VFRoe-ncv (Y, τ, U, e) scheme for coarse meshes. Despite its poor accuracy on coarse meshes (except for α), the latter is quite efficient on very fine meshes. The two VFRoe-ncv (Y, τ, U, P) have very similar performances, with a slight advantage for the energy relaxation method.

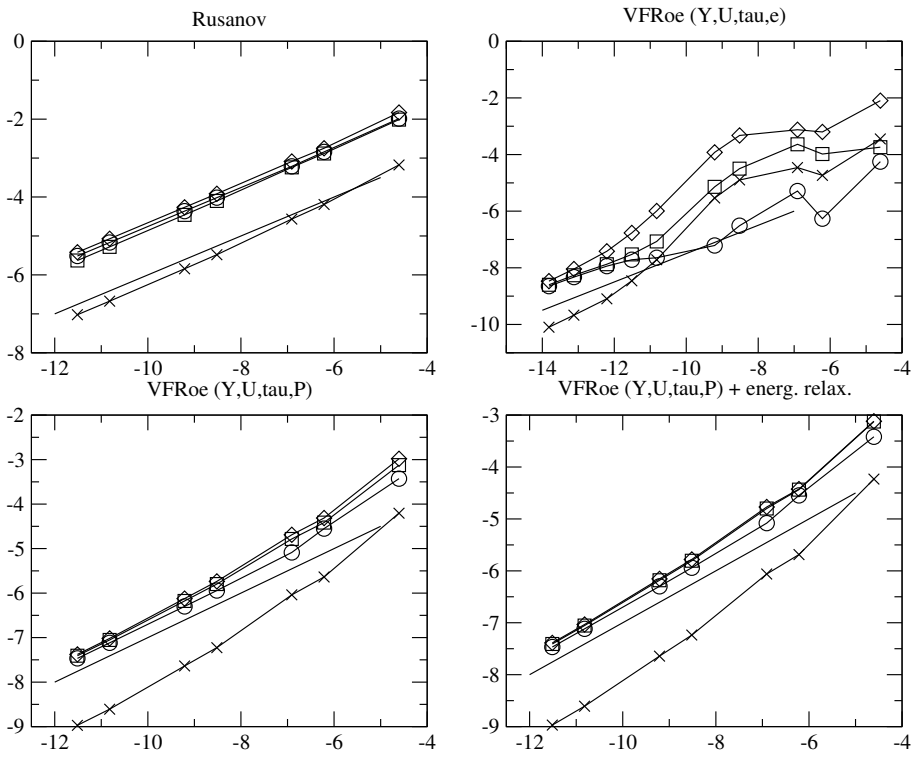

Figure 1: Convergence curves for the test of the section 4.1.1, logarithm of the error (35) versus the logarithm of the mesh size. The meshes contain respectively 10^2, 5 10^2, 10^3, 5 10^3, 10^4, 5 10^4 and 10^5 cells. Additional meshes with 5 10^5, 5 10^5 and 10^6 cells have been used for the VFRoe-ncv (Y, τ, U, e) scheme. The circles correspond to the fractions, the square to the density, the diamond to the velocity and the "X" to the pressure. The plain line represents the slope 1/2.

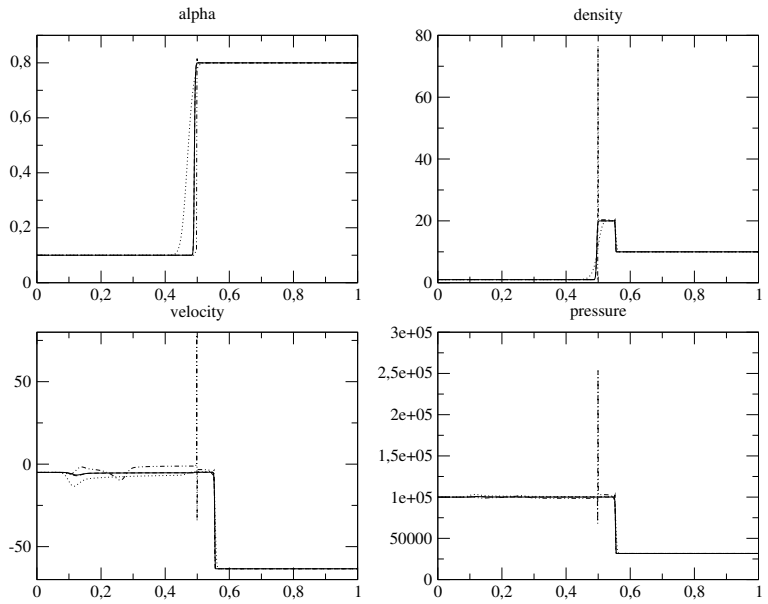

Figure 2: Approximated solutions for $N = 10^3$ obtained with: Rusanov (dot), VFRoe-ncv (Y, τ, U, e) (dot-dash), VFRoe-ncv (Y, τ, U, P) (dash), and VFRoe-ncv (Y, τ, U, P) with energy relaxation (plain line).

4.1.2 Test case with initial conditions of table (14)

Another analytical test case is investigated now. It is also based on the solution proposed in appendix 6.1, but the EOS parameters are those of section 4.3. These parameters are representative of high-pressure high-temperature water and lead to a very stiff mixture where the two phasic EOS parameters strongly differ. In fact the partial derivative of the pressure with respect to the specific volume, $\partial P/\partial \tau$, has an order of magnitude of 10^{15} which corresponds to a very low compressibility. This term is involved in the computation of the flux of the VFRoe-ncv (Y, τ, U, e) scheme and the resulting convection matrix is ill-conditioned. As a consequence, unstable (with respect to time and with respect to the mesh size) oscillations are observed for this scheme, leading to the blow-up of the code for the meshes up to $5\ 10^2$ cells.

The Rusanov scheme, the VFRoe-ncv (Y, τ, U, P) scheme and the VFROE-ncv (Y, τ, U, P) scheme with energy relaxation do not encounter any particular problem to handle this test case. The convergence curves are plotted on figure (6). The VFRoe-ncv (Y, τ, U, e) scheme can not handle this test case for a mesh containing more than $5\ 10^2$ cells and it has thus not been considered here. For the present test case, the final time is small and the contact wave only travels on a distance of $1.46\ 10^{-4}\ m$ to the left. This explains the flatness of the convergence curves for the two VFRoe-ncv schemes on coarse meshes. Indeed, the accuracy does not change until the mesh size becomes of the order of magnitude of $1.46\ 10^{-4}\ m$, which corresponds to a mesh with $6.8\ 10^3$ cells. As shown by figure (6), the order of convergence

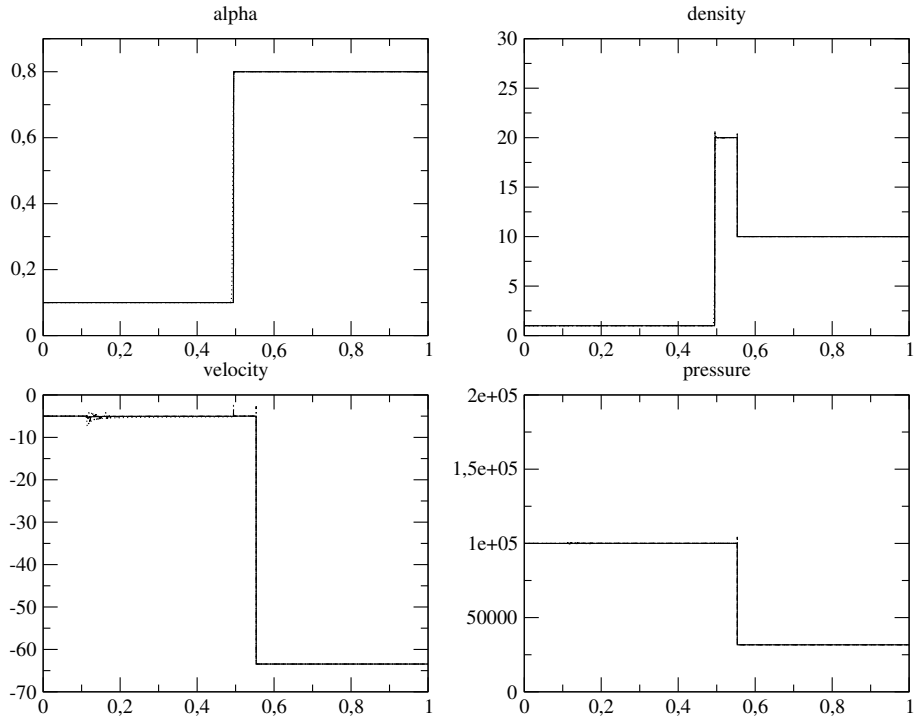

Figure 3: Approximated solutions for $N = 10^5$ obtained with: Rusanov (dot), VFRoe-ncv (Y, τ, U, e) (dot-dash), VFRoe-ncv (Y, τ, U, P) (dash), and VFRoe-ncv (Y, τ, U, P) with energy relaxation (plain line).

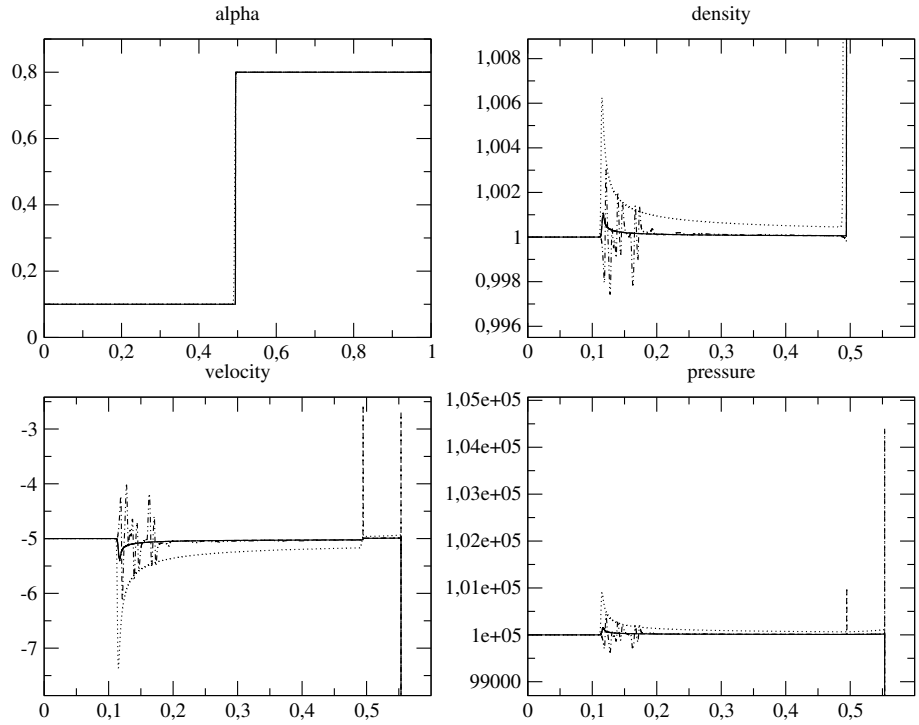

Figure 4: Approximated solutions for $N = 10^5$ obtained with: Rusanov (dot), VFRoe-ncv (Y, τ, U, e) (dot-dash), VFRoe-ncv (Y, τ, U, P) (dash), and VFRoe-ncv (Y, τ, U, P) with energy relaxation (plain line). Zoom on the ghost wave.

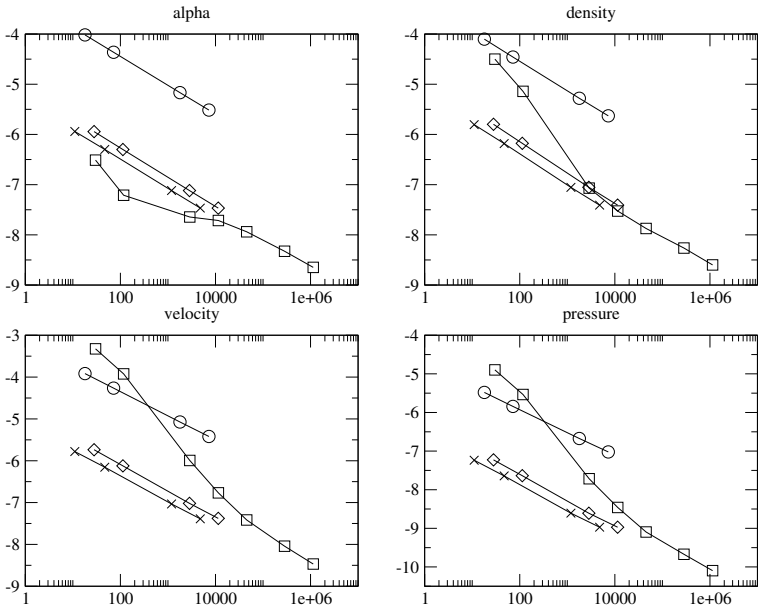

Figure 5: Computational efficiency of the different schemes: error (35) with respect to the CPU time in seconds computed for the meshes $N = \{5\ 10^3, 10^4, 5\ 10^4, 10^5\}$ and with the additional points $N = \{2\ 10^5, 5\ 10^5, 10^6\}$ for the VFRoe-ncv (Y, τ, U, e) scheme. The circles stand for Rusanov, the squares for VFRoe-ncv (Y, τ, U, e), the diamonds for VFRoe-ncv (Y, τ, U, P), and the crosses for VFRoe-ncv (Y, τ, U, P) with energy relaxation.

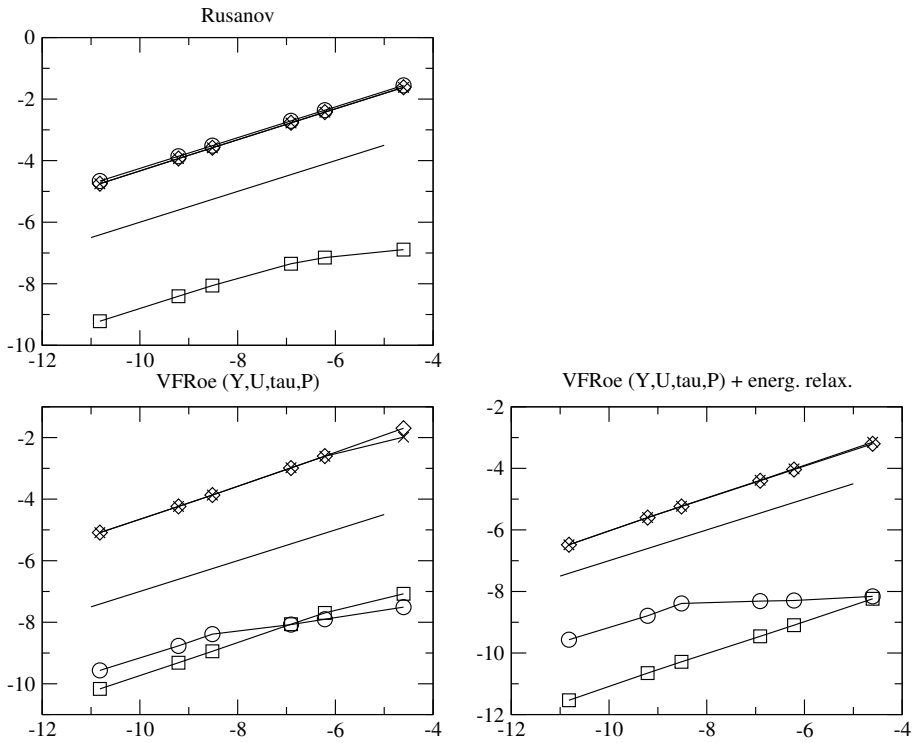

Figure 6: Convergence curves for the test of the section 4.1.2, logarithm of the error (35) versus the logarithm of the mesh size. The meshes contain respectively 10^2, 5 10^2, 10^3, 5 10^3, 10^4 and 5 10^4 cells. The circles correspond to the fractions, the square to the density, the diamond to the velocity and the "X" to the pressure. The plain line represents the slope 1/2.

1/2 is recovered on the finest meshes.

The error (35) versus the computational time in seconds is plotted on the figure (7). It can be noted that the gap between the two VFRoe-ncv (Y, τ, U, P) schemes has increased. Even if the time step can be 3 times greater with the VFRoe-ncv (Y, τ, U, P) scheme with energy relaxation, one time-step costs less CPU-time. Hence the VFRoe-ncv (Y, τ, U, P) scheme with energy relaxation is a more efficient (see appendix 6.3 for a discussion on that point).

Remark. On the basis of theses remarks, the VFRoe-ncv (Y, τ, U, P) schemes seem to be the most appealing for industrial purposes. The VFRoe-ncv (Y, τ, U, P) with energy relaxation has the great advantage to avoid the computation of e with respect to (Y, τ, P), which can be tricky and CPU-consuming when considering real EOS. For complex EOS, the CPU-efficiency between the two schemes would thus probably increase, in favour of the energy relaxation method.

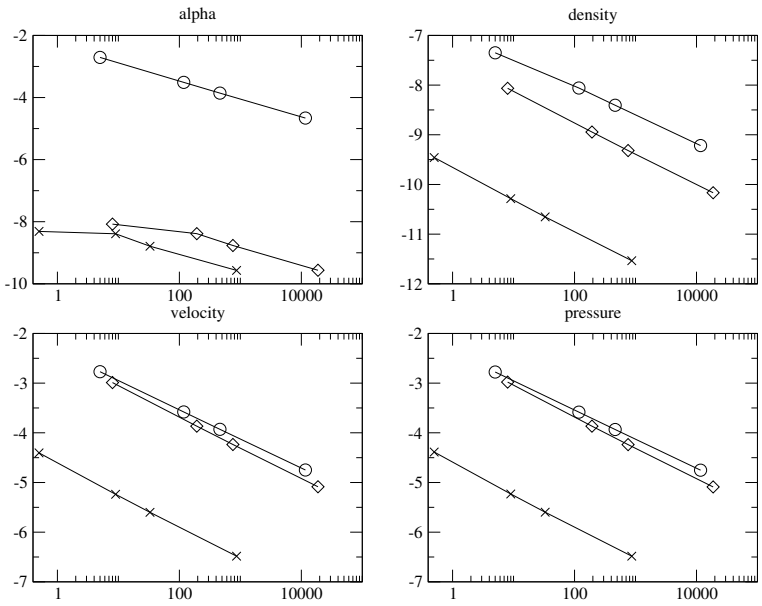

Figure 7: Computational efficiency of the different schemes: error (35) with respect to the CPU time in seconds computed for the meshes $N = \{10^3, 5\ 10^3, 10^4, 5\ 10^4\}$. The circles stand for Rusanov, the diamonds for VFRoe-ncv (Y, τ, U, P), and the crosses for VFRoe-ncv (Y, τ, U, P) with energy relaxation.

4.2 Realistic test cases

4.3 Parameters for the EOS

Stiffened gas EOS (section 3.1) have been retained for each phase. The parameters γ_k, $C_{v,k}$, Π_k and s_k^0 must be specified in order to obtain a satisfactory behaviour. We proceed by defining a reference point in the thermodynamical plane, (P^{ref}, T^{ref}), and by defining the EOS parameters that ensure the equilibrium of the pressure, temperature and chemical potentials of each phase for the reference point (P^{ref}, T^{ref}). When some additional information is needed, as for example the density at (P^{ref}, T^{ref}), we use an industrial thermodynamical tool (tabulated laws). It must be emphasised that the parameters s_k^0 are defined at the end of the procedure: they allow to set the equilibrium of the chemical potentials. Indeed, the other quantities do not depend on s_k^0. Obviously, other methods can be proposed as in [bar05, sau08, liu13].

In the following, all the quantities with a subscript ref are obtained with a thermodynamical tabulated EOS for (P^{ref}, T^{ref}). The subscript m stands for mixture. We are interested in almost single-phase liquid configurations. Hence we can assume that the enthalpy h_m^{ref} and the density ρ_m^{ref} are almost equal to the value of the enthalpy and the density of the liquid phase: $h_m^{ref} \sim h_l^{ref}$ and $\rho_m^{ref} \sim \rho_l^{ref}$.

We intend to perform steam-liquid water simulations so that the vapour can be

modelled by a perfect gas EOS and we thus impose $\Pi_v = 0$. For the vapour, the temperature law (22) and the definition of the phasic sound speed (19) are then:

$$(\gamma_v - 1)\rho_v^{ref} C_{v,v} T^{ref} = P^{ref} \text{ and } \rho_v^{ref} (c_v^{ref})^2 = \gamma_v P^{ref}.$$

Hence, these equations allow to determine γ_v and $C_{v,v}$:

$$\gamma_v = \frac{\rho_v^{ref} (c_v^{ref})^2}{P^{ref}} \text{ and } C_{v,v} = \frac{P^{ref}}{(\gamma_v - 1)\rho_v^{ref} T^{ref}}$$

We now turn to the liquid phase. The phasic sound speed (19), the pressure law (21) and the temperature law (22) give γ_l, Π_l and $C_{v,l}$ respectively:

$$\begin{aligned}
\gamma_l &= 1 + \frac{(c_l^{ref})^2}{h_m^{ref}} \\
\Pi_l &= \frac{\rho_m^{ref} e_m^{ref}(\gamma_l) - P^{ref}}{\gamma_l} \\
C_{v,l} &= \frac{e_m^{ref} - \Pi_l/\rho_m^{ref}}{T^{ref}}
\end{aligned}$$

where $e_m^{ref} = h_m^{ref} - P^{ref}/\rho_m^{ref}$. The parameters s_k^0 only play a role in the chemical potential, and then for the computation of the chemical potential equilibrium, in which they appear as the difference $(s_v^0 - s_l^0)$. We then set $s_l^0 = 0$ and we choose s_v^0 to get small values of the equilibrium fractions (we recall that we have used $\rho_m^{ref} \sim \rho_l^{ref}$, which holds for small fractions). This step is achieved using the equilibrium of the chemical potentials together with the pressure-temperature equilibrium.

This procedure gives the parameters of the phasic EOS and the initial condition of the computations. With the following choices:

$$\begin{aligned}
&P^{ref} = 71.41\ 10^5\ (Pa), \quad T^{ref} = 559.0\ (K), \\
&\rho_v^{ref} = 37.0\ (kg/m^3), \quad c_v^{ref} = 490.0\ (m/s), \\
&h_l^{ref} = 1.3\ 10^6\ (J/kg), \quad \rho_l^{ref} = 739.8\ (kg/m^3), \quad c_l^{ref} = 978.6\ (m/s),
\end{aligned}$$

we get the parameters:

$$\begin{aligned}
&C_{v,v} = 2.3083917370268987\ 10^3\ (J/kg/K), \gamma_v = 1.2542537313432836, \\
&\Pi_v = 0\ (Pa), s_v^0 = -1.85\ 10^4\ (J/kg/K),
\end{aligned}$$

$$\begin{aligned}
&C_{v,l} = 1.3391115339515329\ 10^3\ (J/kg/K), \gamma_l = 1.7366599692307694, \\
&\Pi_l = 4.0046334099937820\ 10^8\ (Pa), s_l^0 = 0\ (J/kg/K),
\end{aligned}$$

and the equilibrium fractions:

$$\begin{aligned}
\alpha_{eq} &= 1.68370180282557914\ 10^{-4}, \\
y_{eq} &= 5.01034544638372543\ 10^{-6}, \\
z_{eq} &= 5.01093788583719112\ 10^{-6}.
\end{aligned}$$

The temperature $T^{ref} = 559\ (K)$ is close to the saturation temperature for the pressure P^{ref}.

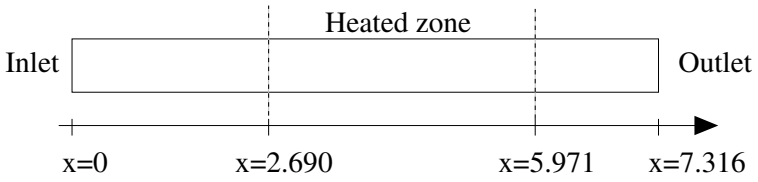

Figure 8: Sketch of the CSNI test case.

4.4 The heating pipe test case

This test case has been the object of the OECD/CSNI benchmark [csni80] and has emerged from discussions in the CSNI working group on Emergency Core Cooling of Water Reactors. It is representative of the cooling of the core of a nuclear power plant and has thus been widely used as a reference test case for the code THYC [lec89] in the 80's. In the present test case, there are two differences with the OECD/CSNI test case. We have our own EOS whereas in the benchmark a EOS is provided. Moreover the heating scenario is different: the heating begins sooner and the maximum of the heating is reached sooner. In fact, the scenario proposed in the benchmark was longer to be sure to start the heating with a stationary state. In our case, the initial condition already corresponds to a stationary state.

As depicted on figure (8), the domain is $x \in [0, 7.316\ m]$. The heating is uniform on the interval $[2.690\ m, 5.971\ m]$ and it starts at $t = 10^{-4}\ s$. The power Φ increases linearly from 0 to $1.4\ 10^6\ W$ during $10^{-3}\ s$. The term Φ represents the source term of the total energy in system (3) and is explicitly integrated. The initial conditions are those described in the previous section with the velocity:

$$U = 1.46845391999612396\ (m/s).$$

We focus on long time simulations with the two VFRoe-ncv (Y, τ, U, P) schemes. Indeed, we are interested in the stationary state which is reached after a few seconds on a coarse mesh, which corresponds to the industrial need. In fact we use here a mesh containing 10^2 uniform cells.

The choice of the time scales λ_i is crucial but we lack of physical information on their value. We thus choose arbitrarily all the time scales $\lambda_i = 10^{-8}\ s$. We recall that, since the λ_i are constant, the numerical scheme for the integration of the source terms is exact whatever the time step is.

The results are plotted for the time $T_{end} = 5\ s$ on figure (9) and the results obtained at the outlet of the pipe are plotted with respect to the time on figure (10). An offset can be observed for the fractions computed by the two schemes. This offset is also quite important for the pressure and the velocity and almost negligible for the density. The origin of the difference has not been clearly identified but some hypothesis can be proposed. First, the inlet state is enforced without considering local Riemann problem and outgoing waves. This method is rough and a more subtle way of computing this inlet state should probably be tested, as the

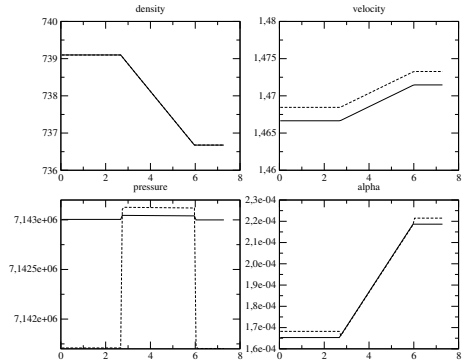

Figure 9: Numerical approximations for the heating pipe test case at time $t = 5\ s$ and for a mesh with 10^2 cells. Plain line: VFRoe-ncv (Y, τ, U, P) scheme with energy relaxation, dashed line: VFRoe-ncv (Y, τ, U, P) scheme

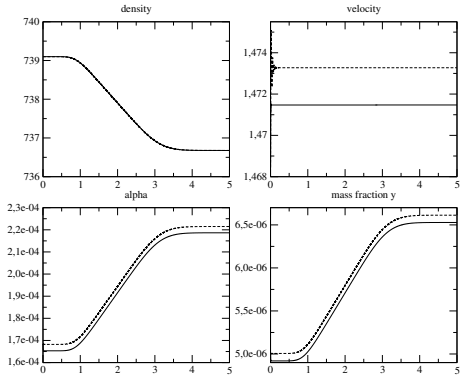

Figure 10: Values at the outlet of the pipe $x = 7.316\ m$ versus the time for the heating pipe test case for a mesh with 10^2 cells. Plain line: VFRoe-ncv (Y, τ, U, P) scheme with energy relaxation, dashed line: VFRoe-ncv (Y, τ, U, P) scheme

classical one proposed in [aud13]. Secondly, considering the mesh size, the time step for the VFRoe-ncv (Y, τ, U, P) has the same order of magnitude as λ_i, whereas for the VFRoe-ncv (Y, τ, U, P) scheme with energy relaxation it is much larger than λ_i. This probably leads to a different (de)coupling of the convection and source effects through the fractional step method.

When focusing on this test case, and using the same CFL constraint of 0.45, the time step for the VFRoe-ncv (Y, τ, U, P) scheme with energy relaxation is 30 times greater than the time step for the VFRoe-ncv (Y, τ, U, P). An obvious consequence is that the total CPU time for the simulation is considerably shorter. We insist that this gain strongly depends on the test case and on the EOS parameters (see appendix 6.3 for some details). It is due to the complex EOS for the mixture and to the relaxation terms. Indeed, when considering a convective case without source terms, it can be recovered that the VFRoe-ncv (Y, τ, U, P) scheme with energy relaxation has a smaller time-step than the VFRoe-ncv (Y, τ, U, P) scheme.

With a more physical point of view, the heating of the steam-water mixture leads to steam creation (the fractions increase). The quantity of steam that is generated remains small. This is probably due to the phasic stiffened gas EOS which may be too simple in this test case. Some stable oscillations can be observed on the velocity at the beginning of the simulation (10), during the transient heating period. They are probably due to the interaction of waves coming upstream from the heating zone with the boundary conditions that are too rough. The amplitude of these oscillations is smaller for the VFRoe-ncv (Y, τ, U, P) scheme with energy relaxation.

5 Conclusion

In the present paper, a complete scheme has been proposed to perform two-phase flow simulations. The underlying model [bar05,hel06] takes into account the pressure, temperature and chemical potential disequilibria. Some interesting features have been exhibited.

- The source terms can be accounted for using an exact integration when considering constant relaxation time scales λ_i. This is an important feature since this allows to handle all the ratios $\lambda_i/\Delta t$, from $\lambda_i/\Delta t \ll 1$ (i.e. almost instantaneous relaxation) to $\lambda_i/\Delta t \gg 1$ (i.e. almost negligible relaxation effects). When the time scales are not constant (i.e. when they depend on the fractions), an exact integration is not always possible and the scheme proposed here gives a first-order approximation of the solution.

- Concerning the convection part of the model, the results obtained with four existing schemes have been compared. The two-phase flow model has a complex non-linear EOS and the following remarks can be made.

  - For VFRoe-ncv schemes, the results confirm that the choice of the set of variables (Y, τ, U, P) must be prefered to the variables (Y, τ, U, e), especially on coarse meshes.
  - For complex EOS, the VFRoe-ncv scheme with energy relaxation can be more efficient that the VFRoe-ncv scheme. In particular, the former avoids to compute complex variable changes that can be expensive in terms of CPU-time. Nevertheless, the overall gain in CPU-time is difficult to foresee and it strongly depends on the test case, on the mesh size and on the EOS parameters.

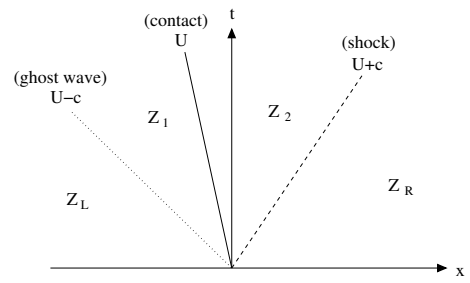

Figure 11: Sketch of the Riemann problem, with a $(U-c)$ ghost-wave and a $(U+c)$-shock.

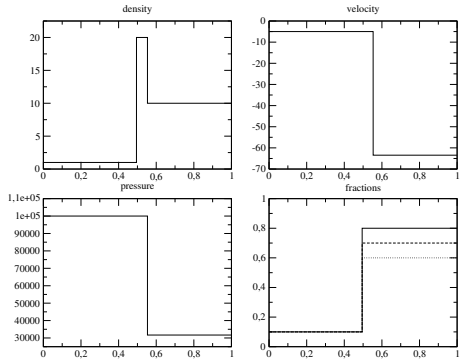

Figure 12: The analytical solution plotted at $t = 0.001\ s$ for the first Riemann problem (13).

6 Appendix

6.1 Analytical solutions for the convection system

We consider here the convective part of the system (3) and we propose to construct an analytical solution of the system for a Riemann problem [god96]. We use a classical technique which consists in choosing the left state, and to define the intermediate states from the left state to the right state. For the sake of simplicity in expression of the solution, we only consider a contact discontinuity and a $(U+c)$-shock. It should be noticed that even if the $(U-c)$-wave is a ghost-wave it leads to a severe test case.

Let us note $Z = (Y, \rho, U, P)$. As depicted in figure (11), Z_L and Z_R denote the left and the right states, Z_1 and Z_2 are the intermediate states. Since the $(U-c)$-wave is a ghost-wave, we obviously have $Z_1 = Z_L$. Through the contact discontinuity the velocity and the pressure are constant: $P_2 = P_1$ and $U_1 = U_2$, and we must specify Y_2 and ρ_2. In order to define Z_R from Z_2 we use the Rankine-Hugoniot relations:

$$\begin{cases} -\sigma[\rho Y] + [\rho U Y] = 0 \\ -\sigma[\rho] + [\rho U] = 0 \\ -\sigma[\rho U] + [\rho U^2 + P] = 0 \\ -\sigma[\rho E] + [\rho U E + U P] = 0 \end{cases} \tag{36}$$

where σ stands for the velocity of the shock and $[\phi] = \phi_R - \phi_2$. We have omitted the jump relations for the fractions since they are obvious and lead to $Y_R = Y_2$. The system (36) yields one degree of freedom, and we choose to specify ρ_R. The system

(36) can be written:

$$\begin{cases} [Y] = 0 \\ J^2 = -\dfrac{[P]}{[\tau]} \\ J = -\dfrac{[P]}{[U]} \\ [e] + [\tau]\dfrac{P_R + P_2}{2} = 0 \end{cases} \tag{37}$$

with $J = \rho(U - \sigma)$, which thanks to the mass equation is such that $[J] = 0$. For a shock wave, J is negative. Since we have chosen to specify ρ_R the third equation of (37) is a resolvant equation for P_R:

$$e(Y_R, \tau_R, P_R) - e(Y_2, \tau_2, P_2) + (\tau_R - \tau_2)\frac{P_R + P_2}{2} = 0 \tag{38}$$

In our particular case, the EOS for the internal energy leads to a non-linear equation for (38) and it must be solved using some classical numerical algorithm (Newton, Quasi-Newton, dichotomy, etc ...). Once P_R is computed, σ and U_R are obtained through relations (37). The first equation of (37) gives J, and then the second equation of (37) gives U_R. The velocity σ is obtained by the relation $J = \rho_R(U_R - \sigma)(= \rho_2(U_2 - \sigma))$.

We apply the previous procedure with the following thermodynamical parameters:

$$C_{v,v} = 2.0, \quad \gamma_v = 1.5, \quad \Pi_v = 1500, \quad C_{v,l} = 1.0, \quad \gamma_l = 1.4, \quad \Pi_l = 1000,$$

and we obtain the states gathered in table (13) (the values in red are those specified, and the values in blue are those that have been computed). The velocity of the $(U + c)$-shock is then equal to $\sigma = 53.4429721063797913$ (m/s). The solution is plotted on the figure (12) at time 0.001 s.

	$Z_L(= Z_1)$	Z_2	Z_R
α	0.1	0.8	0.8
y	0.1	0.7	0.7
z	0.1	0.6	0.6
τ	1.0	0.05	0.1
U	-5.0	-5.0	-63.4429721063797771
P	10^5	10^5	31688.3802274582995

Figure 13: States for the first Riemann problem, the values in red are those specified and the values in blue are those that have been computed from the red values.

When applying the previous procedure with the thermodynamical parameters of the section 4.3 we obtain the states gathered in the table (14) (the values in red are those specified, and the values in blue are those that have been computed). The velocity of the $(U + c)$-shock is then equal to $\sigma = 965.891668252039835$ (m/s). The solution is plotted on the figure (16) at time 7.3 10^{-5} s.

	$Z_L(=Z_1)$	Z_2	Z_R
α	1.68370180282557914 10^{-4}	1.7 10^{-3}	1.7 10^{-3}
y	5.01034544638366529 10^{-6}	5.1 10^{-5}	5.1 10^{-5}
z	5.01093788583713013 10^{-6}	5.1 10^{-5}	5.1 10^{-5}
τ	1.35300183074677709 10^{-3}	1.34228187919463080 10^{-3}	1.35501355013550135 10^{-3}
U	-2.0	-2.0	-11.1805442788134375
P	7141636.39642549586	7141636.39642549586	521736.019901064807

Figure 14: States for the Riemann problem with the EOS parameters of the section 4.3, the values in red are those specified and the values in blue are those that have been computed from the red values.

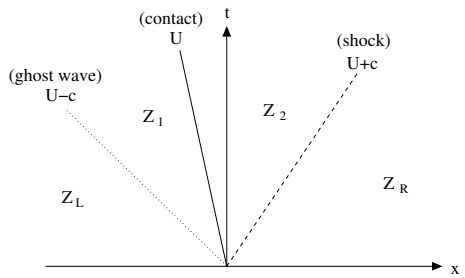

Figure 15: Sketch of the Riemann problem, with a $(U-c)$ ghost-wave and a $(U+c)$-shock.

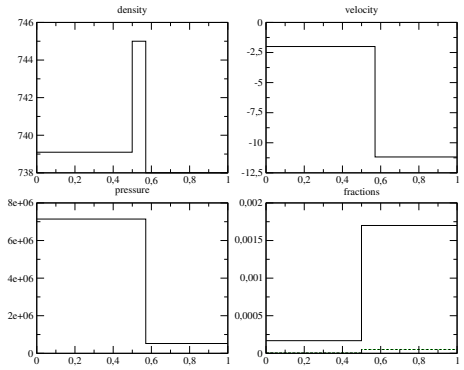

Figure 16: The analytical solution plotted at $t = 7.3\ 10^{-5}\ s$ for the second Riemann problem (14) with the EOS parameters of the section 4.3.

6.2 The vanishing of the energy fraction with stiffened gas EOS

Let us consider two stiffened gas EOS. We now express the pressure and temperature equilibria with definitions (21) and (22):

$$\begin{cases} \frac{z}{\alpha}\frac{e}{\tau}(\gamma_l-1)-\Pi_l\gamma_l = \frac{1-z}{1-\alpha}\frac{e}{\tau}(\gamma_v-1)-\Pi_v\gamma_v \\ \frac{\frac{z}{y}e-\Pi_l\frac{\alpha}{y}\tau}{C_{v,l}} = \frac{\frac{1-z}{1-y}e-\Pi_v\frac{1-\alpha}{1-y}\tau}{C_{v,v}}. \end{cases}$$

We now assume that the energy fraction z is equal to zero but that the volume fraction is not null: $z=0$ and $0<\alpha<1$. The pressure and temperature equilibria respectively lead to:

$$\begin{cases} \frac{e}{\tau} = (1-\alpha)\Pi_v - \frac{C_{v,v}}{C_{v,l}}\Pi_l\frac{(1-y)\alpha}{y}. \\ \frac{e}{\tau} = \frac{(\Pi_v\gamma_v-\Pi_l\gamma_l)(1-\alpha)}{\gamma_v-1}. \end{cases} \tag{39}$$

Hence, the pressure-temperature equilibrium is possible if the two left hand side terms of (39) are equal. This equality is equivalent to defining a mass fraction y

such that:

$$y = \frac{1}{1+A}, \text{ with } A = \frac{C_{v,l}}{C_{v,v}} \frac{\Pi_l - \Pi_v}{\Pi_l} \frac{1-\alpha}{\gamma_v - 1}. \tag{40}$$

Hence, if the parameters Π_k are such that $\Pi_l - \Pi_v > 0$, A is also positive and the fraction y defined by the pressure-temperature equilibrium (40) is defined in $]0,1[$. Moreover, the potential equilibrium can be ensured through the adequate choice of the parameters s_k^0 without modifying (40).

As a consequence, when considering stiffened gas EOS and depending on the choice of the values of the parameters, it is possible to get the equilibrium fractions Y^{eq} such that α^{eq} and y^{eq} are in $]0,1[$ and $z^{eq} = 0$. Further explanations can be found in [jun13].

6.3 Influence of the test case and of the EOS parameters on the time steps

For stiffened gas EOS (see section 3.1), we can exhibit explicitely the two quantites:

$$\Gamma_1 = 1 + \tau \frac{\partial}{\partial e}(P) \quad \text{and} \quad \Gamma_2 = -\frac{\tau}{P}\frac{\partial}{\partial \tau}(P) + \tau \frac{\partial}{\partial e}(P),$$

that appear in the VFRoe-ncv scheme with energy relaxation presented in section 3.2.3. Focusing on the pressure and temperature formula (13) we have:

$$\frac{1}{T}\frac{\partial}{\partial \tau}(P) = \frac{\alpha_v \Pi_v (\alpha_v P_v - z_v P)}{y_v C_{v,v} T_v^2} + \frac{\alpha_l \Pi_l (\alpha_l P_l - z_l P)}{y_l C_{v,l} T_l^2} - \frac{z_v e_v (\gamma_v - 1)}{\tau_v^2 T_v} - \frac{z_l e_l (\gamma_l - 1)}{\tau_l^2 T_l}$$

and

$$\frac{1}{T}\frac{\partial}{\partial e}(P) = \frac{z_v (z_v P - \alpha_v P_v)}{y_v C_{v,v} T_v^2} + \frac{z_l (z_l P - \alpha_l P_l)}{y_l C_{v,l} T_l^2} + \frac{z_v (\gamma_v - 1)}{\tau_v T_v} + \frac{z_l (\gamma_l - 1)}{\tau_l T_l}.$$

These expressions are very complex and it is very difficult to predict the behaviour of Γ_1 and Γ_2 for a given test case. These parameters are used to choose the time step for the VFRoe-ncv scheme with energy relaxation. Numerical simulations have shown different behaviours depending on the test case and on the EOS parameters. In fact, the mixture EOS is very complex and non-linear. The sound of speed c for the mixture strongly depends on the fractions, especially for small fractions for which the derivative of c with respect to the fractions is huge. It has a U-shape and the mixture sound of speed can be less that the sound of speed in each pure phase. It can explain some of the descrepancies observed for the time steps computed for the schemes VFRoe with or without energy relaxation.

The test cases of sections 4.1.1 and 4.1.2 are pure convection problems. In such cases, the time-step of the VFRoe scheme is 3 times greater than the time step of the VFRoe scheme with energy relaxation. In other words, for these cases the wave speeds computed for the VFRoe scheme with energy relaxation bound the wave speeds computed for the VFRoe scheme. The difference of efficiency is then mainly due to the computation of the thermodynamical quantities that is more expensive

for the VFRoe scheme without relaxation. This is more sensitive with the stiff EOS of section 4.1.2 than with the parameters of section 4.1.1.

When turning to test cases involving source terms, as the test case of section 4.1.2, results may become different. In such test cases the interaction between source terms and convection can lead to important differences in the computed fractions, especially on coarse meshes. Due to the dependence of the celerity on the fractions and its U-shape, the computed time steps may become different for the two schemes. For the test case of section 4.1.2 the time-step for the VFRoe scheme is 30 times smaller than that computed for the VFRoe scheme with energy relaxation. The same test case has been examined for a different set of EOS parameters:

$$\begin{array}{ll} C_{v,v} = 2632.943644231272\ (J/kg/K), & \gamma_v = 1.12985176056338, \\ \Pi_v = 0\ (Pa), & s_v^0 = -24952.69807920495\ (J/kg/K), \end{array}$$

$$\begin{array}{ll} C_{v,l} = 85.54318061310099\ (J/kg/K), & \gamma_l = 5.0, \\ \Pi_l = 1.345950717616000\ 10^8\ (Pa), & s_l^0 = 10000\ (J/kg/K), \end{array}$$

and with the initial fractions:

$$\begin{array}{l} \alpha_v = 0.05, \\ y = 0.00263245655737121, \\ z = 0.016644487003907305. \end{array}$$

The time step computed with the VFRoe scheme is then only 4 times smaller than the time-step computed for the VFRoe scheme with energy relaxation.

6.4 Concavity of the mixture entropy

In this section we investigate the concavity of the mixute entropy (12). A less computational demonstration can be found in [jun13]. We assume that each phasic entropy s_k is strictly concave. Thus the Hessian s_k'' of s_k with respect to τ_k and e_k is symmetric definite strictly negative at any point (τ_k, e_k):

$$\forall (\tau_k, e_k) > 0,\ \forall (x_1, x_2) \neq (0,0),\ (x_1, x_2).s_k''(\tau_k, e_k).(x_1, x_2)^\top < 0. \tag{41}$$

Hence we have for $(x_1, x_2) \neq (0,0)$:

$$(x_1, x_2).s_k''(\tau_k, e_k).(x_1, x_2)^\top = x_1^2 \frac{\partial^2 (s_k)}{\partial \tau_k \partial \tau_k} + 2x_1 x_2 \frac{\partial^2 (s_k)}{\partial \tau_k \partial e_k} + x_2^2 \frac{\partial^2 (s_k)}{\partial e_k \partial e_k} < 0.$$

Let us define $\overline{s}_k(\alpha, y, z, \tau, e) = y_k s_k(\frac{\alpha_k \tau}{y_k}, \frac{z_k e}{y_k})$ and $\overline{s}_k''$ the Hessian of $\overline{s}_k$ with respect to (α, y, z, τ, e). It can be shown after some calculus that for any $X = (x_1, x_2, x_3, x_4, x_5)$ we have:

$$\begin{array}{rcl} X.\overline{s}_k''(\alpha, y, z, \tau, e).X^\top & = & X_{a,k}^2 \dfrac{\partial^2 (s_k)}{\partial \tau_k \partial \tau_k} + 2X_{a,k} X_{b,k} \dfrac{\partial^2 (s_k)}{\partial \tau_k \partial e_k} + X_{b,k}^2 \dfrac{\partial^2 (s_k)}{\partial e_k \partial e_k} \\ & + & \xi_k \left(2x_1 x_4\ \frac{P_k}{T_k} + 2x_3 x_5\ \frac{1}{T_k} \right), \end{array} \tag{42}$$

with $\xi_l = 1$, $\xi_v = -1$, and

$$\begin{aligned} X_{a,l} &= \sqrt{y}\left(\tfrac{\tau_l}{\alpha}x_1 - \tfrac{\tau_l}{y}x_2 + \tfrac{\alpha}{y}x_4\right), \\ X_{b,l} &= \sqrt{y}\left(-\tfrac{e_l}{y}x_2 + \tfrac{e_l}{z}x_3 + \tfrac{z}{y}x_5\right), \\ X_{a,v} &= \sqrt{(1-y)}\left(-\tfrac{\tau_v}{1-\alpha}x_1 + \tfrac{\tau_v}{1-y}x_2 + \tfrac{1-\alpha}{1-y}x_4\right), \\ X_{b,v} &= \sqrt{(1-y)}\left(\tfrac{e_v}{1-y}x_2 - \tfrac{e_v}{1-z}x_3 + \tfrac{1-z}{1-y}x_5\right). \end{aligned} \tag{43}$$

We denote by $H_k(X)$ the quadratic part of $X.\overline{s}_k''.X^\top$ at (α, y, z, τ, e):

$$H_k(X) = X_{a,k}^2 \frac{\partial^2(s_k)}{\partial\tau_k\partial\tau_k} + 2X_{a,k}X_{b,k}\frac{\partial^2(s_k)}{\partial\tau_k\partial e_k} + X_{b,k}^2\frac{\partial^2(s_k)}{\partial e_k\partial e_k}$$

Since $s = \overline{s}_l + \overline{s}_v$, the Hessian s'' of s with respect to (α, y, z, τ, e) is $s'' = \overline{s}_l'' + \overline{s}_v''$. Thus, thanks to the concavity of the phasic entropies s_k (41) we have:

$$\forall(\alpha, y, z, \tau, e) \in]0,1[^3\times\mathbb{R}^+,\ \forall X \notin \mathcal{D}_{(\alpha,y,z,\tau,e)}, \quad H_l(X) + H_v(X) < 0.$$

The degeneracy manifold $\mathcal{D}_{(\alpha,y,z,\tau,e)}$ at the point $(\alpha, y, z, \tau, e) \in]0,1[^3\times\mathbb{R}^+$ is the set of $X = (x_1, x_2, x_3, x_4, x_5)$ such that $X \neq 0$ and such that $X_{a,l} = X_{b,l} = X_{a,v} = X_{b,v} = 0$, which gives:

$$\begin{aligned} x_2 &= x_1\tfrac{y(1-y)}{\alpha(1-\alpha)}, \\ x_3 &= x_1\tfrac{z(1-z)}{\alpha(1-\alpha)}, \\ x_4 &= x_1\tau\tfrac{\alpha-y}{\alpha(1-\alpha)}, \\ x_5 &= x_1 e\tfrac{z-y}{\alpha(1-\alpha)}. \end{aligned} \tag{44}$$

using (43). The concavity of the mixture entropy s with respect to the whole variable (α, y, z, τ, e) is thus not easy to investigate.

If we define the function $(\tau, e) \to \nu_{(\alpha,y,z)}(\tau, e) = s(\alpha, y, z, \tau, e)$, then for any $Z = (x_1, x_2) \neq (0, 0)$, the Hessian $\nu''_{(\alpha,y,z)}$ of $\nu_{(\alpha,y,z)}$ is such that:

$$Z.\overline{\nu}''_{(\alpha,y,z)}(\tau, e).Z^\top = \textstyle\sum_{k=l,v}\left(Z_{a,k}^2\dfrac{\partial^2(s_k)}{\partial\tau_k\partial\tau_k} + 2Z_{a,k}Z_{b,k}\dfrac{\partial^2(s_k)}{\partial\tau_k\partial e_k} + Z_{b,k}^2\dfrac{\partial^2(s_k)}{\partial e_k\partial e_k}\right), \tag{45}$$

with

$$Z_{a,l} = \tfrac{\alpha}{\sqrt{y}}x_4, \quad Z_{b,l} = \tfrac{z}{\sqrt{y}}x_5, \quad Z_{a,v} = \tfrac{1-\alpha}{\sqrt{(1-y)}}x_4, \quad Z_{b,v} = \tfrac{1-z}{\sqrt{(1-y)}}x_5. \tag{46}$$

It can be noted that the degeneracy manifold associated to $\nu''_{(\alpha,y,z)}$ is thus empty. Thanks to (41) this implies that the function $\nu_{(\alpha,y,z)}$ is strictly concave.

We now focus on the definition of the equilibrium fractions (9). Let us define the function $(\alpha, y, z) \to \eta_{(\tau,e)}(\alpha, y, z) = s(\alpha, y, z, \tau, e)$. It can be shown that for any $V = (v_1, v_2, v_3)$ the Hessian $\eta''_{(\tau,e)}$ of $\eta_{(\tau,e)}$ satisfies:

$$V.\eta''_{(\tau,e)}(\alpha, y, z).V^\top = \textstyle\sum_{k=l,v}\left(V_{a,k}^2\dfrac{\partial^2(s_k)}{\partial\tau_k\partial\tau_k} + 2V_{a,k}V_{b,k}\dfrac{\partial^2(s_k)}{\partial\tau_k\partial e_k} + V_{b,k}^2\dfrac{\partial^2(s_k)}{\partial e_k\partial e_k}\right), \tag{47}$$

with

$$\begin{aligned} V_{a,l} &= \sqrt{y}\left(\tfrac{\tau_l}{\alpha}v_1 - \tfrac{\tau_l}{y}v_2\right), \\ V_{b,l} &= \sqrt{y}\left(-\tfrac{e_l}{y}v_2 + \tfrac{e_l}{z}v_3\right), \\ V_{a,v} &= \sqrt{(1-y)}\left(-\tfrac{\tau_v}{1-\alpha}v_1 + \tfrac{\tau_v}{1-y}v_2\right), \\ V_{b,v} &= \sqrt{(1-y)}\left(\tfrac{e_v}{1-y}v_2 - \tfrac{e_v}{1-z}v_3\right). \end{aligned} \tag{48}$$

Thus, thanks to the concavity of the phasic entropies s_k (41) we have:

$$\forall(\alpha,y,z) \in]0,1[^3,\ \forall V \notin \mathcal{D}'_{(\alpha,y,z)}, \quad V.\eta''_{(\tau,e)}(\alpha,y,z).V^\top < 0.$$

The degeneracy manifold $\mathcal{D}'_{(\alpha,y,z)}$ at the point $(\alpha,y,z) \in]0,1[^3$ is the set of $V = (v_1,v_2,v_3)$ such that $V \neq 0$ and such that $V_{a,l} = V_{b,l} = V_{a,v} = V_{b,v} = 0$, which using (48) gives:

$$v_1 = v_2 = v_3 \quad \text{and} \quad \alpha = y = z.$$

As a consequence, if the three fractions are not equal $\mathcal{D}'_{(\alpha,y,z)}$ is empty; and when $\alpha = y = z$ the degeneracy manifold is $\mathcal{D}'_{(\alpha,y,z)} = \{v \neq 0, v(1,1,1)\}$. The latter situation may lead to the non-uniqueness of the equilibrium fraction (9) if $\mathcal{D}'_{(\alpha,y,z)}$ is not empty when the gradient of $\eta_{(\tau,e)}$ vanishes. If we assume that $\alpha_{eq} = y_{eq} = z_{eq}$, we have $e_l = e_v = e$, $\tau_l = \tau_v = \tau$ and relations (14), (15) and (16) give the system:

$$\left\{\begin{array}{l} T_l(\tau,e) = T_v(\tau,e), \\ P_l(\tau,e) = P_v(\tau,e), \\ \mu_l(\tau,e) = \mu_v(\tau,e), \end{array}\right. \Leftrightarrow \left\{\begin{array}{rcl} \dfrac{\partial}{\partial\tau_l}(s_l)(\tau,e) &=& \dfrac{\partial}{\partial\tau_v}(s_v)(\tau,e), \\ \dfrac{\partial}{\partial e_l}(s_l)(\tau,e) &=& \dfrac{\partial}{\partial e_v}(s_v)(\tau,e), \\ s_l(\tau,e) &=& s_v(\tau,e). \end{array}\right. \tag{49}$$

Hence system (49) has no solution if there does not exist a point (τ,e) such that the two phasic entropies and their derivative coincide. Eventually, if (49) has no solution the degeneracy manifold $\mathcal{D}'_{(\alpha,y,z)}$ is empty when the gradient of $\eta_{(\tau,e)}$ vanishes. Since the function $\eta_{(\tau,e)}$ is concave with respect to (α,y,z), it implies that $\eta_{(\tau,e)}$ is strictly concave when the gradient of $\eta_{(\tau,e)}$ vanishes. In such a case, the equilibrium fraction (9) is thus unique.

7 Bibliography

[all07] Allaire G., Faccanoni G., Kokh S., (2007), "A strictly hyperbolic equilibrium phase transition model", C. R. Acad. Sci. Paris, Vol. 344 pp. 135–140.
[ath07] "Steam ATHOS/SGAP 3.1. Analysis of Thermal Hydraulics of Steam Generators/Steam Generator Analysis Package, Version 3.1, Volume 1, Mathematical and Physical Models and Method of Solution". EPRI, Palo Alto report, CA: 2007.1016564.
[aub88] Aubry S., Cahouet J., Lequesne P., Nicolas G., Pastorini S., (1988), "THYC Code de Thermohydraulique des Coeurs de Racteurs Version 1 .0. Modélisation et Méthodes Numériques". EDF internal report HT-13/8886 A (in french).
[aud13] Blondel F., Audebert B., Pasutto T., Stanciu M., (2013), "Condensation models and boundary conditions for non-equilibrium wet steam flows". Int. J. of Finite Volumes, Vol. 10 pp. 1–53.
[bar05] Barberon T., Helluy P., (2005), "Finite volume simulation of cavitating flows". Computers and Fluids, Vol. 34 pp. 832–858.
[buf00] Buffard T., Gallouët T., Hérard J.-M., (2000), "A sequel to a rough Godunov scheme: application to real gases". Computers and Fluids, Vol. 29 pp. 813–847.
[car04] Caro F., (2004), "Modélisation et simulation numérique des transitions de phase liquide-vapeur", PhD. Thesis Ecole Polytechnique (France),
http://pastel.archives-ouvertes.fr/pastel-00000993.
[coq98] Coquel F., Perthame B., (1998), "Relaxation of energy and approximate Riemann solvers for general pressure laws in fluid dynamics equations". SIAM J. Numer. Anal., Vol. 35(6) pp. 2223-2249. In Memory of Ami Harten.
[dow96] Downar-Zapolski P., Bilicki Z., Bolle L., Franco J., (1996), "The non-equilibrium relaxation model for one-dimensional flashing liquid flow ". International Journal of Multiphase Flow, Vol. 22 pp. 473–483.
[eym00] R. Eymard, T. Gallouët, R. Herbin, (2000), "The finite volume method". Handbook for Numerical Analysis, Ph. Ciarlet J.L. Lions eds, North Holland, 715-1022.
[fac08] Faccanoni G., (2008), "Étude d'un modèle fin de changement de phase liquide-vapeur. Contribution à l'étude de la crise d'ébullition.", PhD. thesis Ecole Polytechnique (France) and Di Trento University (Italy),
http://tel.archives-ouvertes.fr/tel-00363460.
[fac12] Faccanoni G., Kokh S., Allaire G., (2012), "Modelling and Simulation of Liquid-Vapor Phase Transition in Compressible Flows Based on Thermodynamical Equilibrium". Math. Mod. and Num. Analysis, Vol. 46 pp. 1029–1054.
[fau00] Faucher E., Hérard J.-M., Barret M., Toulemonde C., (2000), "Computation of Flashing Flows in Variable Cross-Section Ducts", Int. J. of Comp. Fluid Dynamics, Vol. 13 pp. 365–391.
[gal96] Gallouët T., Masella J.-M., (1996), "Un schéma de Godunov approché". Comptes rendus de l'Académie des Sciences (Paris), Vol. I-323 pp. 77–84.
[gal02a] Gallouët T., Hérard J.-M., Seguin N., (2002), "Some recent finite volume schemes to compute Euler equations using real gas EOS". Int. J. Numer. Meth. Fluids, Vol. 39 pp. 1073–1138.
[gal02b] Gallouët T., Hérard J.-M., Seguin N., (2002), "A hybrid scheme to compute

contact discontinuities in one dimensional Euler systems". Math. Mod. and Num. Analysis, Vol. 36 pp. 1133-1159.
[gal03] Gallouët T., Hérard J.-M., Seguin N., (2003), "On the use of some symmetrising variables to deal with vacuum". Calcolo, Vol. 40 pp. 163-194.
[gav07] Gavrilyuk S., Saurel R., (2007), "Rankine-Hugoniot relations for shocks in heterogeneous mixtures", J. of Fluid Mech., Vol. 575 pp. 495–507.
[gue03] Guelfi A., Pitot S., (2003), "THYC (ThermoHYdraulique des Composants) Version 4.1 - Note de Principe". EDF internal report HI-84-03-020A (in french).
[gui05] Guillard H., Murrone A., (2005), "A five equation reduced model for compressible two phase flow problems". Journal of Computational Physics, Vol. 202 pp. 664-698.
[god96] Godlewski E., Raviart P.-A., (1996), "Numerical analysis for hyperbolic systems of conservation laws". Springer Verlag.
[hel06] Helluy P., Seguin N., (2006), "Relaxation models of phase transition flows", Math. Mod. and Num. Analysis, Vol. 40(2) pp. 331–352.
[hel10] Helluy P., Hérard J.-M., Mathis H., Müller S., (2010), "A simple parameter-free entropy correction for approximate Riemann solvers". Comptes Rendus Mécanique, Vol. 388 pp. 493–498.
[hel11] Helluy P., Mathis H., (2011), "Pressure laws and Fast Legendre Transform", Math. Models Methods Appl. Sci., Vol. 21(4) pp. 745–775.
[jun13] Jonathan Jung, (2013), "Schémas numériques adaptés aux accélérateurs multicoeurs pour les écoulements bifluides". PhD. Thesis Strasbourg University (France),
http://tel.archives-ouvertes.fr/tel-00876159.
[kap01] Kapila A. K., Menikoff R., Bdzil J. B., Son S. F., Stewart D. S., (2001), "Two-phase modeling of deflagration-to-detonation transition in granular materials: Reduced equations", Phys. of Fluids, Vol. 13 pp.3002–3024.
[kar58] Karplus H.B., (1958), "The velocity of sound in a liquid containing gas bubbles". Armour Research Foundation Project No. A-097.
[lec89] Le Coq G., Aubry S., Cahouet J., Lequesne P., Nicolas G., Pastorini S., (1989), "The THYC computer code. A finite volume approach for 3 dimensional two-phase flows in tube bundles". EDF Bulletin de la direction des Etudes et Recherche - Série A, Nucléaire. Hydraulique. Thermique, Vol. 1 pp. 61–76.
[liu13] Liu Y., (2013), "Contribution à la vérification et à la validation d'un modèle diphasique bifluide instationnaire", PhD Thesis Aix-Marseille University (France).
[mas99] Masella J.-M., Faille I., Gallouët T., (1999), "On an approximate Godunov scheme". Int. J. of Comp. Fluid Dynamics, Vol. 12 pp. 133–149.
[mat10] Mathis H., (2010), "Etude théorique et numérique des écoulements avec transition de phase", PhD. Thesis Strasbourg University (France),
http://tel.archives-ouvertes.fr/tel-00516683.
[rus61] Rusanov V.V., (1961). "Calculations of interaction of non-steady shock waves with obstacles". J. Comp. Math. Phys., Vol. 1 pp. 267–279.
[sau08] Saurel R., Petitpas F., Abgrall R., (2008). "Modelling phase transition in metastable liquids: application to cavitating and flashing flows". J. Fluid Mech., Vol. 607 pp. 313–350.

[tou95] Toumi I., (1995), “FLICA IV : Manuel de référence. Méthode numérique”. CEA internal report DMT93/439.
[wal69] Wallis G.B., (1969), “One-dimensional two-phase flow”. McGraw-Hill.
[csni80] Werner W., (1980), “First CSNI numerical benchmark problem. Comparison report”. CSNI report 47.
[yan68] Yanenko N. N., (1968), “Méthodes à pas fractionnaires”. Armand Colin.